1

2 **Brain-wide connectivity patterns of feedforward and feedback cortico-cortical neurons in**

3 **the mouse secondary visual cortex**

4

5 Richard G. Dickson[1], Matthew W. Jacobs[1], John M. Ratliff[1], Alec L.R. Soronow[1], Faye An[1],

6 Walid A. Yuqob[1], Euiseok J. Kim[1,2,3]*

7 [1]Department of Molecular, Cell, and Developmental Biology, University of California, Santa

8 Cruz, CA 95064, USA

9 [2]Institute for the Biology of Stem Cells, University of California, Santa Cruz, CA 95064, USA

10 [3]Lead Contact

11

12 Running title: Brain-wide circuits for FF/FB neurons

13

14

15

16

17

18 *Corresponding Author: Euiseok J. Kim

19 Department of Molecular, Cell, and Developmental Biology, University of California, Santa

20 Cruz, 1156 High Street, Santa Cruz, CA 95064, USA

21 Phone: 831-502-7233

22 Fax: 831-459-3139

23 ekim62@ucsc.edu

24

ACKNOWLEDGEMENTS

We thank Bin Chen, Bradley Colquitt, and David Feldheim for reading the manuscript and Efrain Hernandez Alvarez for mouse husbandry and histology. We thank undergraduate volunteers Eugene Kim, Jordan Chong, Hannah Tao, Lily Taylor-Hunt, Paul Pham, and Julian Swartz for tissue processing and histology. We acknowledge technical support from Benjamin Abrams, UCSC Life Sciences Microscopy Center, RRID: SCR_021135. Purchase of the Zeiss 880 confocal microscope used in this research was made possible through the National Institutes of Health s10 Grant 1S10OD23528-01. We acknowledge support from the UCSC start-up fund, the Whitehall Foundation, the Hellman Fellows Program, the E. Matilda Ziegler Foundation for the Blind, BRAIN Initiative at the National Institutes of Health RF1MH132591 and the National Institute of Neurological Disorders and Stroke at the National Institutes of Health, R01NS128771 (E.J.K.), the Koret scholar program (A.L.R.S.), and a National Institutes of Health IRACDA Postdoctoral Training Grant, K12GM139185 (R.G.D.).

ABSTRACT

Feedforward and feedback cortico-cortical neurons are distinct yet spatially intermingled subtypes distributed across cortical layers, playing specialized roles in sensory and cognitive processing. However, whether their presynaptic inputs differ to support these functions remains unknown. Using projection- and layer-specific monosynaptic rabies tracing, we mapped brain-wide long-distance inputs to multiple feedforward and feedback neuron types in VISl (also known as LM), the mouse secondary visual cortex. Overall, long-distance input patterns for these feedforward and feedback neurons were largely similar, as all received the majority of their inputs from VISp, the primary visual cortex, along with substantial inputs from various other cortical and visual thalamic regions. Despite their similarities, these feedforward and feedback types differed in the proportion of long-distance cortical inputs originating from specific visual, retrosplenial, and auditory cortices. These findings reveal the input connectivity patterns of cortico-cortical neurons based on feedforward and feedback projections, providing an anatomical framework for future studies on their functions and circuit integration.

KEYWORDS

cortical hierarchy, cortico-cortical neurons, feedforward and feedback neurons, mouse visual cortex, rabies tracing

KEY POINTS

1) Feedforward and feedback cortico-cortical projection neurons in VISl form largely distinct populations that are distributed across multiple cortical layers.

2) Four different feedforward and feedback cortico-cortical projection neuron types receive broadly similar patterns of long-distance input across the brain.

63 **3)** Despite overall similarities, feedforward and feedback neurons differ in the relative

64 proportions of inputs from specific areas, including visual, retrosplenial, and auditory cortices.

INTRODUCTION

The mammalian cortex is responsible for high-level perception and cognition and is composed of numerous interconnected cortical areas (Felleman and Van Essen, 1991; Oh et al., 2014; Gămănuţ et al., 2018). These areas communicate through long-distance inter-areal connections mediated by excitatory cortico-cortical projection neurons (CCPNs). Two key organizational features of the mammalian cortex are its six-layered laminar structure and its hierarchical organization (Felleman and Van Essen, 1991; Cajal, 1995). Each cortical layer is considered as a different information-processing unit (Harris and Shepherd, 2015). CCPNs in a specific layer of each cortical area can be further divided into feedforward projection neurons, which send axons to higher-order cortical areas, and feedback projection neurons, which project to lower-order cortical areas. These two neuronal types are thought to process distinct types of information, feedforward neurons primarily transmitting sensory input from the external world and feedback neurons modulating contextual factors such as attention, brain states, and background information (Hupé et al., 1998; Nassi et al., 2013; Keller et al., 2020; Debes and Dragoi, 2023). Despite their distinct roles, these feedforward and feedback neurons are spatially intermingled within cortical layers (Berezovskii et al., 2011). Recent advances have elucidated their functional roles (Keller et al., 2020; Fişek et al., 2023), however, it remains unclear whether feedforward and feedback projection neurons within a specific layer of a given cortical area receive distinct or similar brain-wide presynaptic inputs. Uncovering this would provide insight into their proposed functional differences.

The mouse visual cortex serves as an ideal model for investigating the brain-wide connectivity of layer- and projection-specific cell types at a cellular level. This is due to the availability of viral genetic tools that enable precise labeling of neurons based on their axonal projections (e.g., retrograde tracer such as AAVretro) and laminar identity (e.g., layer-specific Cre-expressing

89 transgenic mouse lines) (Gerfen et al., 2013; Tervo et al., 2016; Chatterjee et al., 2018; Matho et
90 al., 2021). Additionally, the hierarchical organization of mouse visual cortical areas has been
91 well characterized both anatomically and functionally (Harris et al., 2019; Siegle et al., 2021;
92 D'Souza et al., 2022). The mouse visual cortex comprises the primary visual cortex (VISp) and
93 at least ten different higher visual areas (HVAs), including the lateromedial (VISl) and
94 posteromedial (VISpm) visual cortices (Wang and Burkhalter, 2007). In the cortical hierarchy,
95 VISp represents the lowest level, VISl occupies an intermediate position, and VISpm is at a
96 higher level (Harris et al., 2019; D'Souza et al., 2022). Within this framework, CCPNs in VISl
97 that project to VISpm are defined as feedforward neurons, whereas those projecting to VISp are
98 defined as feedback neurons (D'Souza et al., 2022). This makes VISl particularly suitable for
99 studying spatially intermingled feedforward and feedback CCPNs.

100 Previous studies have mapped the monosynaptic inputs of layer-specific excitatory neuronal
101 types (Vélez-Fort et al., 2014; DeNardo et al., 2015; Kim et al., 2015, 2020; Yao et al., 2023a).
102 These studies suggest that long-distance input connectivity to specific layer-defined neuronal
103 classes can be either distinct or largely comparable and that local connectivity varies (DeNardo
104 et al., 2015; Yao et al., 2023a). However, it remains unclear whether feedforward and feedback
105 CCPNs within the same cortical layer receive distinct brain-wide monosynaptic inputs,
106 highlighting a critical gap in our understanding of cortical circuit organization.

107 To investigate the brain-wide monosynaptic input connectivity of layer-specific feedforward and
108 feedback CCPNs in the mouse visual cortex, we employed the intersectional G-deleted rabies
109 tracing method - cTRIO (cell-type specific inputs and outputs relationship) (Schwarz et al.,
110 2015). Using an intersectional approach that combined layer-specific Cre recombinase with
111 projection-specific tTA trans-activator expression, we defined distinct subtypes of feedforward
112 and feedback CCPNs in layer 2/3 (L2/3) and 5 (L5) of VISl. We then mapped their long-distance

113 monosynaptic inputs using rabies tracing, leveraging two avian receptors, TVA and TVA^{66T}, for
114 avian sarcoma leukosis virus glycoprotein EnvA (Wickersham et al., 2007; Miyamichi et al.,
115 2013). Thus we are able to trace the monosynaptic inputs to neuronal subtypes which were
116 previously inaccessible to brainwide mapping efforts. Our findings reveal that while the overall
117 input patterns to L2/3 and L5 feedforward and feedback CCPNs in VISl are largely comparable,
118 there are notable differences in the proportions of long-distance inputs from the visual, auditory,
119 and retrosplenial cortices. The experimental design presented here provides a framework for
120 investigating hierarchical brain-wide networks across different species and brain structures
121 beyond the mouse visual cortex. This study also provides a comprehensive presynaptic input
122 connectivity map that will serve as a foundation for future experimental and theoretical
123 investigations into cortico-cortical neuronal functions.
124

125 **MATERIALS AND METHODS**

126 **Resource and materials availability**

127 Further information and requests for resources and materials should be directed to and will be
128 fulfilled by the lead contact, Euiseok J. Kim (ekim62@ucsc.edu). Microscopy and any additional
129 data reported in this paper will be shared by the lead contact upon reasonable request.
130

131 **Experimental animals**

132 GENSAT BAC transgenic *SepW1-Cre* NP39 and *Tlx3-Cre* PL56 mouse lines have been
133 previously described (Gerfen et al., 2013). The transgenic mice were maintained on C57BL/6J
134 backgrounds. C57BL/6J mice were used as wild-type. Both male and female mice were used. All
135 mice were housed with a 12-hour light and 12-hour dark cycle and *ad libitum* access to food and

136 water. All animal procedures were performed in accordance with the University of California,
137 Santa Cruz animal care and use committee (IACUC)'s regulations.
138
139 **Virus preparation**
140 All adeno-associated viruses (AAVs) and SAD B19 EnvA-pseudotyped glycoprotein (G)-deleted
141 rabies virus (EnvA+RVdG) were produced by the Salk Viral Core GT3: scAAVretro-hSyn-BFP
142 ($1.26X10^{12}$ GC/ml), scAAVretro-hSyn-H2B-eGFP ($1.16X10^{13}$ GC/ml), scAAVretro-hSyn-H2B-
143 mCherry ($1.21X10^{13}$ GC/ml), AAVretro-nEF-lox66/71-tTA ($4.8X10^{13}$ GC/ml), AAV8-TRE-
144 DIO-oG ($5.92X10^{12}$ GC/ml), AAV8-TRE-DIO-eGFP-T2A-TVA ($7.00X10^{13}$ GC/ml), AAV8-
145 TRE-DIO-TVA^{66T}eGFP-P2A-oG ($7.40X10^{13}$ GC/ml), and EnvA+RVdG-mCherry ($7.71X10^{8}$-
146 $1.43X10^{10}$) Infectious Unit (IU)/ml).
147
148 **Animal surgery for virus injection**
149 For all surgeries anesthesia induction was with 100 mg/kg of ketamine and 10 mg/kg of xylazine
150 cocktail via intraperitoneal injections, and anesthesia was maintained as needed with ~1%
151 isoflurane. Mice were mounted in a stereotax (RWD instruments) for surgery and stereotaxic
152 injections. For rabies tracing experiments, *SepW1-Cre* NP39 or *Tlx3-Cre* PL56 mice received
153 AAV helper injections at postnatal day (P)63-P125. 50-200 nl of AAVretro-nEF-lox66/71-tTA
154 was injected into the center of the medial secondary visual cortex (VISpm), primary visual
155 cortex (VISp), or anterior cingulate area (ACA) using the following coordinates: 1.6 mm rostral,
156 1.5 mm lateral relative to lambda and 0.4-0.6 mm ventral from the pia for VISpm or 1.1 mm
157 rostral, 2.6 mm lateral to lambda and 0.45-0.67 mm ventral from the pia for VISp, 0.4 mm
158 rostral, 0.4 mm lateral to bregma and 0.7-0.8 mm ventral from the pia for ACA. A 50 nl mixture
159 of 9:1 AAV8-TRE-DIO-oG and AAV8-TRE-DIO-eGFP-T2A-TVA, a 50 nl mixture of 2:7:1

160 AAV8-TRE-DIO-oG, 1x PBS and AAV8-TRE-DIO-eGFP-T2A-TVA, or 50 nl of AAV8-TRE-
161 DIO-TVA^{66T}eGFP-P2A-oG was injected into the center of the lateral secondary visual cortex
162 (VISl), using the following coordinates: 0.7 mm rostral, 3.65 mm lateral relative to lambda and
163 0.4-0.6 mm ventral from the pia. We injected AAVs using air pressure using a 1 ml syringe with
164 18G tubing adaptor and tubing. To prevent virus backflow, the pipette was left in the brain for 5-
165 10 minutes after the completion of the injection. After recovery, mice were given water with
166 ibuprofen (30 mg/kg) and subcutaneous carprofen (5 mg/kg). Two weeks after AAV helper
167 injection, 100 nl of EnvA+RVdG-mCherry was injected into the same site in VISl using a 1 ml
168 syringe-mediated air pressure. After recovery, mice were again given water with ibuprofen (30
169 mg/kg) and subcutaneous carprofen (5 mg/kg) and housed for seven days to allow for trans-
170 synaptic rabies spread and fluorescent protein expression.

171 For retrograde colocalization studies, mice were prepared and head-fixed as previously with the
172 same coordinates for VISpm, VISp, and ACA as above. For triple AAV colocalization
173 experiments, combination of 50-100 nl of scAAVretro-hSyn-BFP, scAAVretro-hSyn-H2B-
174 mCherry, scAAVretro-hSyn-H2B-eGFP were injected into one of VISp, VISpm, and ACA.
175 AAV was left to express for 18-21 days before the tissue harvest and histology. For
176 VISpm/VISp/ACA chemical tracer colocalization experiments, 50-100 nl of cholera toxin
177 subunit B (CTB) conjugated to Alexa fluor 647 (CTB-647, 1 mg/ml, Invitrogen C34778), Alexa
178 fluor 555 (CTB-555, 1 mg/ml, Invitrogen C22843) and/or Alexa fluor 488 (CTB-488, 1 mg/ml,
179 Invitrogen C34775) was injected into VISpm, VISp, and/or ACA. Three to six days later, the
180 tissue was harvested for histology. Different fluorophore colors were rotated between the three
181 injection sites across different animals. Detailed information of injections on individual mice can
182 be found in Table 1.
183

184 **Histology and image analysis**

185 Brains were harvested after trans-cardiac perfusion using phosphate-buffered saline (PBS)
186 followed by 4% paraformaldehyde (PFA). Brains were dissected out from skulls and post-fixed
187 with 2% PFA and 15% sucrose in PBS at 4°C overnight and then immersed in 30% sucrose in
188 PBS at 4°C before sectioning. Using a freezing microtome, 50-100 µm coronal brain sections
189 were cut and stored in cryogen (30% ethylene glycol, 30% glycerol, 30% ddH_20, 10% 10x PBS)
190 at 4°C, every other section was stained and mounted for data analysis and quantification. Before
191 staining, sections were washed 3x 10 minutes in PBS and permeabilized and blocked in PBS/5%
192 normal donkey serum (Millipore S30-100ML)/1% Triton-X 100 (Sigma-Aldrich X100-100ML)
193 for two hours at room temperature. To enhance eGFP and mCherry signals, free-floating sections
194 were incubated at 4°C overnight with goat anti-GFP (1:1000; Rockland 600-101-215,
195 RRID:AB_218182) and rabbit anti-dsRed (1:500; Clontech 632496, RRID:AB_10013483)
196 primary antibodies in PBS/0.5% normal donkey serum/0.1% Triton-X 100, followed by 3x 10
197 minutes in PBS wash and incubation with the appropriate secondary antibodies conjugated with
198 Alexa 488 or 568 (1:500; Invitrogen A-11055 (RRID:AB_2534102) or A-10042
199 (RRID:AB_2534017), respectively). Sections were counterstained with 10 µM DAPI (4',6-
200 diamidino-2-phenylindole) in PBS for 30 minutes to visualize cell nuclei, followed by 3x 10
201 minutes in PBS wash. Immunostained tissue sections were mounted on slides with a polyvinyl
202 alcohol mounting medium containing DABCO (PVA-DABCO) and allowed to air-dry overnight.

203 All sections were scanned with a 10x/0.45 NA (wd-2.0 mm) objective on a Zeiss AxioImager Z2
204 Widefield Microscope using tile scan and Z-stack (every 6-8 µm). Representative images were
205 taken with the Zeiss 880 Confocal Microscope with 10x/0.45 NA (wd-2.0 mm) or 40x/ 0.95 NA
206 corr (wd-0.25 mm) objectives. Scanned images were first processed in Zeiss ZEN 3.11 with
207 DAPI images for alignment and fluorescent images for eGFP+ or mCherry+ cell detections

208 exported for processing. Subsequent image files were processed and analyzed using Bell Jar for
209 long-distance input mapping (Soronow et al., 2025). For alignment, the center Z-stack DAPI
210 images were used to predict the section's xy coordinates and cut angle for alignment to the Allen
211 Brain Common Coordinate Framework reference atlas (Wang et al., 2020). Alignments were
212 then fine-tuned in Bell Jar to ensure fit and minimize counting rabies-labeled cells resulting from
213 minor TVA expression leakage in non-Cre-expressing neurons (Wall et al., 2010). Layers for
214 VISpm and VISp were also manually fine-tuned to ensure accuracy. The exported Zeiss ZEN
215 files with mCherry+ signals were used for automated cell counting. Using Bell Jar, max
216 projection images were produced from the Z-stacks, and these max projections were then
217 sharpened in the program before detection. Detection thresholds were kept stable unless manual
218 counting validation showed less than 90% accuracy of cell labeling, in which case the confidence
219 interval was adjusted (three out of 15 brains) to ensure accurate counting. Cell detection and
220 brain alignment were then integrated, and the long-distance ipsi-hemispheric cortical input
221 fractions were calculated and graphed using GraphPad Prism 10.1.1. For thalamic input
222 proportions, areas and cells were drawn and counted manually on Zeiss ZEN 3.11 using the
223 Allen Brain Common Coordinate Framework reference atlas (Wang et al., 2020).

224 For VISpm/VISp/ACA CTB colocalization experiments, all CTB labeled cells were counted
225 manually due to weaker fluorescent signals that could not reliably be detected using Bell Jar's
226 automated cell detection. For each animal, three sections corresponding to the same three VISl
227 containing plates from the Allen CCFv3 were selected for counting. Using Fiji, VISl and laminar
228 borders were drawn over DAPI images, cells were labelled individually and then overlayed
229 labels were checked for co-localization.
230

231 **Quantification and Statistical analysis**

232 The values of n and what n represents are reported in results and figure legends. For statistical
233 significance, two-way ANOVA with Tukey's multiple comparisons test was performed with
234 GraphPad Prism 10.1.1. A one-way ANOVA with the Fisher's Least Significant Difference
235 (LSD) post hoc for multiple comparisons test was performed using IBM SPSS 30. Unless
236 otherwise noted, statistical significance is indicated as follows: *$p < 0.05$; **$p < 0.01$; ***$p <$
237 0.001; ****$p < 0.0001$. In Fig. 4C, significance is denoted differently: *(black) $p < 0.05$ and
238 *(magenta) $p < 0.01$.
239
240 **RESULTS**
241 **Feedforward and feedback cortico-cortical projection neurons of VISl are largely non-**
242 **overlapping and distributed across layers**
243 We first investigated the long-distance projection targets of CCPNs in VISl using published data
244 from the Allen Mouse Brain Connectivity Atlas (Harris et al., 2019). This dataset provides high-
245 resolution maps of eGFP+ axonal projections in adult mouse brains, generated by injecting
246 AAV1-CAG-FLEx-eGFP into Cre-expressing transgenic mice to label specific neuronal
247 populations in different brain regions. To examine CCPNs in VISl, we analyzed data from *Cux2-*
248 *IRES-Cre* and *Tlx3-Cre* mice, which label layers 2-4 (L2-4) and L5 CCPNs, respectively. Whole-
249 brain projection maps revealed that both L2-4 and L5 CCPNs extend axons to more than 13
250 cortical areas, including visual areas as VISp, VISpm, and VISpor and non-visual areas such as
251 the temporal association cortex (TEa) and the anterior cingulate area, dorsal part (ACAd) (Fig.
252 1A-B). Quantitative analysis of the axonal projection volumes across these regions showed that
253 L2-4 and L5 CCPNs exhibit similar projection patterns, with the highest projection volume in
254 VISp (39.43 ± 3.20% in *Cux2-IRES-Cre* and 29.75 ± 3.80% in *Tlx3-Cre*, mean ± SEM),
255 followed by VISpm, VISpor, VISli, and VISrl (Fig. 1B). Notably, L2-4 CCPNs exhibit sparse

256 axonal projections to ACAs (1.10 ± 0.28%), whereas 3.55 ± 0.95% of the total axonal
257 projections from L5 CCPNs target ACAd (Fig. 1B).

258 Next, we investigated whether CCPNs in VISl that project to three major cortical target areas
259 (VISp, ACA/MOs (secondary motor cortex), and VISpm) represent distinct or overlapping cell
260 types at the single-cell level. To retrogradely label these projection neurons with three different
261 fluorescent markers, we stereotaxically injected AAVretro-hSyn-H2B-mCherry into VISp,
262 AAVretro-hSyn-BFP into ACA/MOs, and AAVretro-hSyn-H2B-eGFP into VISpm in wild-type
263 adult C57BL/6J mice (Fig. 1C). Thus, VISl neurons projecting to VISpm, VISp, and ACA/MOs,
264 designated as VISl→VISpm, VISl→VISp, and VISl→ACA, respectively. In VISl of these mice,
265 labeled CCPNs were distributed across layers 2-6. The majority of neurons were labeled by a
266 single fluorescent protein (VISl→VISpm: 90.97 ± 2.08%; VISl→VISp: 92.25 ± 5.04%;
267 VISl→ACA: 87.94 ± 4.60%, n = 2 mice) with relatively few exhibiting double or triple labeling
268 (Fig. 1C). These findings indicate that CCPNs projecting to VISpm or ACA/MOs (feedforward,
269 FF) and VISp (feedback, FB) do not extensively share axonal collaterals consistent with a
270 previous study (Berezovskii et al., 2011).
271 To evaluate whether this observation is consistent when using chemical tracers that avoid
272 potential viral co-transduction effects of AAVretros, we stereotaxically injected 50 nl of cholera
273 toxin subunit B (CTB) conjugated to Alexa Fluor 647, 555, or 488 into the ACA, VISp, and
274 VISpm, respectively, alternating fluorophores across animals. In VISl of these triple CTB
275 injected mice, most neurons were labeled by a single fluorescent CTB (VISl→ACA: 75.11 ±
276 10.04%; VISl→VISp: 95.93 ± 1.06%; VISl→VISpm: 85.00 ± 12.92%, n= 4 mice), with
277 relatively few neurons exhibiting double or triple labeling (Fig. 1E, F). In a separate set of
278 experiments, we injected 100 nl of CTB conjugated to Alexa Fluor 647 or 555 into VISp or
279 VISpm, respectively, to maximize labeling of neurons projecting to these areas while minimizing

280 unintended spread to adjacent regions. Even under these double injection conditions, the majority
281 of VISl neurons were labeled by a single fluorescent CTB (VISl→VISp: 94.40 ± 1.05%;
282 VISl→VISpm: 94.95 ± 0.87%, n=3 mice) (Fig. 1E). Therefore, our results indicate that
283 VISl→VISpm, VISl→VISp, and VISl→ACA CCPNs are largely distinct neuronal
284 subpopulations.
285 CCPNs are distributed across all cortical layers from L2/3 to L6. To determine the laminar
286 distribution of the three VISl CCPN types projecting to ACA, VISp, and VISpm, we quantified
287 their soma locations as percentages across layers (Fig. 1G). All three types were present
288 throughout L2-6, with the highest proportions in L5 (VISl→ACA: 41.50 ± 8.62%; VISl→VISp:
289 31.82 ± 3.97%; VISl→VISpm: 45.07 ± 7.29%; n = 3 mice, Fig. 1G). Notably, VISl→ACA
290 CCPNs were more abundant in the upper division of L2/3 ($L2/3^{upper}$) compared to the lower
291 division ($L2/3^{lower}$) (28.56 ± 3.91% vs. 9.08 ± 5.48%, Fig. 1G). VISl→VISpm CCPNs showed a
292 similar trend, with higher proportions in $L2/3^{upper}$ than $L2/3^{lower}$ (12.29 ± 1.77% vs. 7.93 ±
293 2.87%, Fig. 1G). In contrast, VISl→VISp CCPNs were more abundant in $L2/3^{lower}$ compared to
294 $L2/3^{upper}$ (14.66 ± 2.67% vs. 9.58 ± 3.40%, Fig. 1G). Despite these laminar differences, all three
295 CCPN types displayed substantial overlap across the full depth of L2/3 and within L5.
296

297 **Brain-wide monosynaptic input mapping of feedforward and feedback CCPNs in VISl**

298 We examined whether long-distance inputs to feedforward and feedback neurons align with one
299 of three possible organizational models (Fig. 2A). In Model 1, these neurons receive inputs from
300 the same areas they project to, establishing a reciprocal connectivity pattern that facilitates
301 looped computations. In Model 2, feedforward and feedback neurons differ in the type of
302 information they relay; feedforward neurons preferentially receive inputs from lower sensory
303 areas such as VISp and the dorsal lateral geniculate nucleus of the thalamus (LGd), while

304 feedback neurons receive inputs from higher cortical areas that convey contextual information
305 such as higher cortical areas and the lateral posterior thalamic nucleus (LP). In Model 3, both
306 feedforward and feedback neurons receive inputs from the same brain regions, making them
307 anatomically indistinguishable. In this scenario, despite similar long-distance anatomical inputs,
308 feedforward and feedback neurons may exhibit distinct functional roles due to differences in
309 local circuit computations. Alternatively, the long-distance inputs themselves may differ
310 functionally, even if their anatomical connectivity proportion from each brain region appears
311 similar.

312 To differentiate between these three models, we mapped and characterized the brain-wide long-
313 distance inputs to distinct feedforward and feedback CCPNs in VISl. We implemented an
314 intersectional rabies tracing strategy called cTRIO to map monosynaptic inputs in a projection-
315 and layer-specific manner. We first injected a helper virus mixture of AAV8-TRE-DIO-oG
316 (rabies glycoprotein) (Kim et al., 2016) and AAV8-TRE-DIO-eGFP-T2A-TVA into VISl, along
317 with AAVretro-nEF-lox66/71-tTA (hereafter AAVretro-tTA) into projection targets, including
318 VISpm, VISp, and ACA, in L2/3-specific *SepW1-Cre* or L5 CCPN-specific *Tlx3-Cre* transgenic
319 mice (Gerfen et al., 2013). This ensured Cre- and tTA-dependent expression of the avian TVA
320 receptor and rabies glycoprotein (oG). This approach enabled selective labeling of feedforward
321 and feedback neurons in L2/3 or L5 (Fig. 2D). 14 days later, EnvA-pseudotyped glycoprotein
322 (G)-deleted rabies virus (EnvA+RVdG)-mCherry was injected into the same VISl location to
323 enable monosynaptic input tracing from the starter neurons. After seven days, brains were
324 harvested, sectioned, immunostained with goat anti-eGFP (Rockland 600-101-215,
325 RRID:AB_218182) and rabbit anti-dsRed (Clontech 632496, RRID:AB_10013483) antibodies,
326 and imaged to quantify brain-wide long-distance inputs.
327

328 **Control experiments to optimize layer- and projection-specific monosynaptic rabies tracing**
329 We conducted a series of experiments to optimize our monosynaptic rabies tracing approach.
330 Our goal was to minimize false-positive long-distance labeling and prevent contamination of the
331 starter neuron population. Such issues could arise from 'leaky' expression of transgenes such as
332 TVA and oG independent of Cre and tTA activity (Wall et al., 2010; Lavin et al., 2020), as well
333 as from unintended damage to long-distance axonal tracts in the white matter (Watakabe and
334 Hirokawa, 2018) (Fig. 3).

335 To examine the absence of false-positive long-distance rabies labeling, we first injected AAV8-
336 TRE-DIO-eGFP-T2A-TVA (without oG) into VISl and AAVretro-tTA into VISp of *Tlx3-Cre*
337 mice (Fig. 3A). 14 days later, we administered EnvA+RVdG-mCherry into VISl and harvested
338 the brains seven days post-injection (Fig. 3A). As expected, in the absence of oG, no mCherry+
339 rabies-labeled neurons were detected outside of the injection site (VISl) (Fig. 3B-B').

340 In additional controls, we injected either a mixture of AAV8-TRE-DIO-eGFP-T2A-TVA and
341 AAV8-TRE-DIO-oG (Fig. 3C), or AAV8-TRE-DIO-TVA^{66T}eGFP-P2A-oG alone (Fig. 3E) into
342 VISl or VISp, but without AAVretro-tTA injections. In both cases, following EnvA+RVdG-
343 mCherry and a seven-day incubation period, no mCherry+ rabies-labeled neurons outside of the
344 injection site (Fig. 3C-D', E-F')

345 Next, to assess the purity of starter neurons and verify whether L2/3 or L5 VISl→VISp CCPNs
346 contained only VISl→VISp neurons, we injected AAV8-TRE-DIO-TVA^{66T}eGFP-P2A-oG into
347 VISl and a mixture of AAVretro-tTA and Alexa Fluor 647-conjugated cholera toxin subunit B
348 (CTB) into VISp of *Tlx3-Cre* mice (Fig. 3G-H), and collected brains three weeks later. Confocal
349 imaging showed that TVA^{66T}eGFP-P2A-oG labeled L5 neurons in VISl were also labeled with
350 CTB, showing that they were VISl→VISp neurons (Fig. 3H).

351 To determine whether VISl→VISpm neurons were included in the L2/3 VISl→VISp starter
352 population due to passing axons in the grey matter of lower cortical layers (Watakabe and
353 Hirokawa, 2018), we injected AAV8-TRE-DIO-TVA^{66T}eGFP-P2A-oG into VISl, AAVretro-tTA
354 into VISp, and CTB into VISpm of *SepW1-Cre* mice (Fig. 3I-J). Confocal images of brain
355 sections harvested three weeks later showed that TVA^{66T}eGFP-P2A-oG expressing neurons were
356 not labeled with CTB, indicating that virus-labeled starter neurons did not include VISl→VISpm
357 neurons (Fig. 3J). These experiments validate our approach, ensuring specificity in identifying
358 monosynaptic inputs while preventing false positives and potential starter population
359 contamination.

360 **Long-distance cortical inputs onto four different CCPN types in VISl**

361 We examined whether the four types of feedforward and feedback CCPNs (L2/3 VISl→VISpm,
362 L2/3 VISl→VISp, L5 VISl→VISpm, L5 VISl→VISp) in VISl receive similar or distinct
363 monosynaptic inputs from other cortical areas within the ipsilateral hemisphere (Fig. 4 and Table
364 2). Rabies-labeled long-distance input neurons to those four types of CCPNs were distributed
365 throughout both visual and non-visual cortical areas (Fig. 4A), with the highest proportion
366 originating from VISp (L2/3 VISl→VISpm 0.409 ± 0.046, L2/3 VISl→VISp 0.380 ± 0.030, L5
367 L5 VISl→VISpm 0.492 ± 0.016, L5 VISl→VISp 0.582 ± 0.023, Fig. 4B). We quantified and
368 ranked the top 20 cortical regions contributing inputs along the cortical hierarchy (Harris et al.,
369 2019). While overall input patterns among the four CCPN types were largely similar, we
370 identified key differences. L5 VISl→VISp feedback neurons received a greater proportion of
371 long-distance inputs from VISp compared to L5 VISl→VISpm feedforward neurons (Fig. 4B).
372 Similarly, L2/3 VISl→VISpm feedforward neurons received a significantly greater proportion of
373 their inputs from VISpm than L2/3 VISl→VISp feedback neurons (Fig. 4C).

374 Further statistical analysis using one-way ANOVA revealed that at least one of the four CCPN
375 types exhibited a significantly different proportional input than other CCPNs in eight out of the
376 20 cortical areas analyzed (Fig. 4C): VISpm, VISpl, AUDd, AUDp, RSPv, RSPagl, RSPd, and
377 MOs. Overall, these findings suggest that while the four CCPN types receive broadly
378 comparable long-distance cortical inputs, they exhibit distinct preferences for specific cortical
379 regions, reflecting their functional roles in cortical processing. Notably, L5 VISl→VISpm
380 CCPNs receive proportionally more retrosplenial cortex input, suggesting a greater role in visuo-
381 spatial memory, and L2/3 CCPNs regardless of projection receive proportionally more auditory
382 cortex input suggesting a greater role for L2/3 CCPNs in audio-visual integration (Fig. 4B-C).

383 We next investigated the laminar distribution of long-distance presynaptic inputs from VISp and
384 VISpm to four distinct types of feedforward and feedback CCPNs in VISl. Although prior
385 studies have reported preferential long-distance connectivity between superficial layers and
386 between deep layers (DeNardo et al., 2015; Kim et al., 2015), it remains unclear whether CCPNs
387 in specific layers of a given cortical area receive layer-specific long-distance inputs, depending
388 on their feedforward or feedback projections. To address this, we quantified the proportion of
389 input neurons across each layer of VISp and VISpm (Fig. 5A-B) for four distinct CCPN types in
390 VISl: L2/3 VISl→VISpm, L2/3 VISl→VISp, L5 VISl→VISpm, and L5 VISl→VISp. With a
391 few exceptions, the laminar distribution of input neurons in VISp and VISpm did not reveal
392 statistically significant differences across these neuronal groups (Fig. 5A-B).

393 We investigated whether feedforward neurons in VISl that project to cortical areas with higher
394 hierarchy scores than VISpm exhibit more distinct input connectivity patterns from those of
395 VISl→VISp compared to VISl→VISpm neurons. Previous studies have shown that the cortical
396 hierarchy in rodents is relatively shallow compared to that of primates (Harris et al., 2019;

397 D'Souza et al., 2022). The hierarchy scores based on layer-termination patterns of cortico-
398 cortical connection (Harris et al., 2019) for select cortical areas are as follows: VISp: -0.239,
399 VISl: -0.148, VISpm: 0.074, ACAd: -0.060, ACAv: 0.404, and MO: 0.282., To determine if the
400 shallow hierarchy in the mouse visual cortex was masking hierarchy dependent input differences,
401 we injected AAVretro-tTA into ACA/MOs and a mixture of AAV8-TRE-DIO-oG and AAV8-
402 TRE-DIO-eGFP-T2A-TVA into VISl of *Tlx3-Cre* mice to label VISl→ACA/MOs (hereafter,
403 VISl→ACA) neurons and traced their monosynaptic inputs across the cortex. We then compared
404 these results with monosynaptic input tracing of L5 VISl→VISpm feedforward neurons and L5
405 VISl→VISp feedback neurons (Fig. 5C). We found broadly similar input connectivity profiles
406 across these three L5 CCPN subtypes. Thus, the input connectivity of L5 VISl→ACA CCPNs is
407 comparable to that of VISl→VISpm CCPNs and does not exhibit greater differences from
408 VISl→VISp CCPNs than from VISl→VISpm CCPNs. Notably, the proportion of inputs from
409 VISp to VISl→VISp neurons was higher than that to VISl→VISpm and VISl→ACA neurons
410 (Fig. 5C).

411 **Long-distance thalamic input neuron profiles onto four different CCPN types in VISl**

412 Next, we examined whether the four types of feedforward and feedback CCPNs in VISl receive
413 distinct presynaptic inputs from visual thalamic regions. In the mouse visual system, LGd
414 projects to VISl and other higher visual cortical areas in addition to VISp, while LP and the
415 laterodorsal nucleus of the thalamus (LD) also provide input to VISl and other visual cortical
416 regions (Bienkowski et al., 2019).

417 In rabies-traced brain sections, we identified three thalamic nuclei, LGd, LD, and LP, and
418 quantified the proportion of rabies-labeled neurons among all these input areas (Fig. 6A). Across
419 all four CCPN types, LP provided the majority of thalamic inputs, followed by LGd and LD,

420 consistent with a previous study (Yao et al., 2023a) (Fig. 6B). While the overall proportions of
421 thalamic inputs were similar, we observed that L2/3 VISl→VISpm neurons received a lower
422 proportion of inputs from LGd compared to L5 VISl→VISpm neurons (L2/3 VISl→VISpm:
423 0.102 ± 0.008 and L5 VISl→VISpm 0.323 ± 0.027, p=0.0030, two-way ANOVA with Tukey's
424 multiple comparisons test) (Fig. 6B). Conversely, L2/3 VISl→VISpm neurons received a higher
425 proportion of inputs from LP than L5 VISl→VISpm neurons (L2/3 VISl→VISpm 0.887 ± 0.004,
426 L5 VISl→VISpm 0.657 ± 0.024, p=0.0021, two-way ANOVA with Tukey's multiple
427 comparisons test) (Fig. 6B).

428

429 **DISCUSSION**

430 Using a layer- and projection-specific monosynaptic rabies tracing approach, we mapped brain-
431 wide inputs to five distinct types of feedforward and feedback CCPNs in VISl. This study
432 provides the first comprehensive connectivity maps to investigate the organizational principles
433 governing feedforward and feedback neurons in relation to their laminar positions and the
434 hierarchical positions of their target areas. Our findings indicate that long distance input
435 connectivity patterns are largely comparable across CCPN subtypes, supporting Model 3 (Fig.
436 2A), but notable differences emerge based on their laminar and projection identities. First, L2/3
437 VISl→VISpm CCPNs received a higher proportion of inputs from their own projection target,
438 VISpm, compared to L2/3 VISl→VISp and other L5 CCPNs. Similarly, L5 VISl→VISp CCPNs
439 received a higher proportion of inputs from VISp, their projection target, compared to L5
440 VISl→VISpm or VISl→ACA CCPNs. These results are in accordance with Model 1 (Fig. 2A),
441 in which monosynaptic inputs preferentially originate from the neurons' axonal targets (Kim et
442 al., 2020; Siu et al., 2021). These insights provide a foundation for future functional and
443 theoretical studies aimed at understanding brain-wide cortical computations at the cellular level.

444 The input-output organization of neural networks provides crucial insights into the information
445 they receive and the signals they transmit for functional processing. Therefore, understanding
446 neuronal connectivity patterns is essential for a comprehensive understanding of neural circuit
447 function and computation (Zeng and Sanes, 2017). Previous studies have demonstrated that
448 distinct neuronal cell types in the mammalian brain exhibit characteristic input connectivity
449 patterns. Even within broader neuronal classes, spatially intermingled subtypes display subtype-
450 specific input connectivity (e.g., dopaminergic D1 receptor versus D2 receptor expressing spiny
451 projection neurons in the striatum or serotonergic neuron subtypes in the dorsal raphe; see also
452 whole-brain rabies tracing data) (Wall et al., 2016; Ren et al., 2018). A recent study found that
453 functionally distinct neuronal types in layer 2/3 of the mouse somatosensory cortex exhibit
454 distinct brain-wide input connectivity patterns (Inácio et al., 2025). For cortico-cortical
455 connectivity in the visual cortices, a previous study found that VISp CCPNs projecting to VISpm
456 or VISal received inputs from the same respective areas, suggesting a like-to-like connectivity
457 pattern (Kim et al., 2020). A previous study observed laminar differences in like-to-like
458 connectivity using Channelrhodopsin-2-assisted circuit mapping, where there is stronger like-to-
459 like connectivity in L5 compared to L2/3 neurons (Young et al., 2021). This observation of like-
460 to-like connectivity is further supported by a study in macaques, where V1 neurons projecting to
461 V2 receive monosynaptic feedback inputs from V2 but not from other V1-projecting areas (Siu
462 et al., 2021). In the mouse VISl, the secondary visual cortex, projection-specific input
463 connectivity is observed, though it appears less pronounced than in CCPNs of VISp, the primary
464 visual cortex. One possible explanation is that VISl→VISpm and VISl→VISp neurons share
465 similar medial axonal projection trajectories, whereas VISp→VISpm and VISp→VISal (VISp
466 CCPNs projecting to anterolateral, AL, visual cortex) neurons exhibit medial versus lateral
467 projection patterns. Another, not mutually exclusive, possibility is that the cortical hierarchy in

468 the mouse visual system is relatively shallow, making it more challenging to detect strong
469 hierarchical connectivity features.

470 Although little is known about LP and LGd projections to VISl, our observed LP:LGd input
471 ratios are largely consistent with previous rabies-tracing data examining thalamic inputs to layer-
472 specific VISl populations (Yao et al., 2023a). Notably, we found that VISl L5 FF neurons
473 projecting to VISpm receive proportionally more LGd input compared to their L2/3 counterparts,
474 suggesting a Model 2 input organization in which FF neurons receive stronger input from
475 feedback-associated areas such as LGd. However, this pattern is not observed in L2/3 FF
476 neurons, indicating a non-symmetrical input organization between FF and FB neurons across
477 layers. Importantly, our data describe input proportions rather than functional strengths; future
478 quantitative and functional studies, such as electrophysiological recordings or other synaptic
479 connectivity measures, will be necessary to clarify the strength and dynamics of these
480 thalamocortical connections.

481 To validate the projection identities of our starter neurons, we performed CTB injections into
482 both target and non-target projection areas (Fig. 3G-J). However, given the collateralization
483 properties of some CCPNs (Han et al., 2018; Peng et al., 2021), it is possible that a subset of
484 starter neurons also projects to additional areas beyond the intended targets. Notably, axonal
485 reconstructions and RNA barcode-based mapping (MAPseq) by Han et al. demonstrated that
486 approximately 88% of VISp CCPNs project to only one or two of the six higher visual areas.
487 Similarly, Berezovskii et al. (2011) using dextran amine tracers reported that FF (to VISp) and
488 FB (to VISal) CCPNs in VISl are largely non-overlapping, with less than 5% overlap. Our
489 observations of VISl axonal collateralization are consistent with these findings, while
490 acknowledging potential differences between VISl and VISp as well as variations in
491 experimental approaches. Nonetheless, we note that potential collateral projections of VISl

492 CCPNs to areas beyond ACA, VISp, and VISpm could introduce variability in rabies tracing
493 results and complicate efforts to restrict analyses exclusively to single projection-defined
494 populations.

495

496 Monosynaptic rabies tracing is a powerful approach for mapping anatomical connections across
497 the brain; however, this method does not provide information about synaptic strength or other
498 functional properties of these connections (Callaway and Luo, 2015). For example, although
499 feedforward and feedback CCPNs may receive similar proportions of inputs from a given area, it
500 remains unclear whether these input neurons are functionally distinct—for example, whether
501 they exhibit different receptive field properties or belong to different functional subtypes. To
502 gain additional insight into the functional differences and similarities between feedforward and
503 feedback CCPNs, future studies could complement rabies tracing with electrophysiological or
504 imaging approaches. Additionally, advances in high-throughput molecular profiling, including
505 single-cell RNA sequencing, have revealed that cortical neurons within a single layer can be
506 further classified into distinct subtypes based on unsupervised clustering (Tasic et al., 2018; Yao
507 et al., 2023b). Beyond their broad excitatory versus inhibitory or laminar identities, it would be
508 valuable to examine whether long-distance input neurons exhibit specific connectivity patterns
509 among these molecularly defined subtypes of CCPNs (Condylis et al., 2022).

510 It is also possible that, despite receiving similar long-distance inputs, feedforward and feedback
511 neurons differ in their local circuit architecture. To further test Model 3 (Fig. 2A) and uncover
512 additional anatomical distinctions, future studies using TVA^{66T}-dependent rabies tracing for local
513 inputs, combined with molecular characterization of input neurons and electrophysiological
514 profiling would be informative.

515 In this study, we used feedforward (to VISpm or ACA) and feedback (to VISp) CCPNs in VISl
516 as a model to investigate connectivity differences. Given that mammalian visual cortical areas
517 are organized into dorsal and ventral streams with strong intra-stream connectivity, mapping
518 inputs to feedforward and feedback neurons targeting areas within a stream, such as POR, a
519 higher-order ventral stream area, could offer valuable insights (D'Souza et al. 2022; Harris et al.
520 2019). Although POR represents an informative target for examining feedforward and feedback
521 connectivity, precise stereotaxic targeting remains technically challenging. Future studies
522 including POR could further clarify ventral stream-specific connectivity. Another key question
523 for future research is whether similar connectivity profiles would be observed in other cortical
524 regions, such as secondary somatosensory cortex projecting to primary somatosensory cortex as
525 feedback CCPNs and secondary somatosensory cortex projecting to primary and secondary
526 motor cortices as feedforward CCPNs (Yamashita et al., 2018). Given that the cortical hierarchy
527 in mice is relatively shallow compared to that of higher mammals (Harris et al., 2019; D'Souza
528 et al., 2022), it would also be interesting to explore these questions in species with a more robust
529 hierarchical organization, such as marmosets or macaques.
530

531 **Declaration of Interests**

532 The authors declare no competing interests that could have influenced the contents of this
533 publication.
534

535 **Author Contributions**

536 Richard G. Dickson performed investigations, supervised students, collected and curated data,
537 analyzed data, prepared visualizations, and contributed to writing the original draft and revisions.
538 Matthew W. Jacobs performed investigations, supervised students, and collected data. John M.

Ratliff performed investigations, collected and analyzed data, and contributed to writing and revisions. Alec L. R. Soronow performed investigations. Faye An and Walid A. Yuqob collected and analyzed data. Euiseok J. Kim conceived and designed the study, supervised the project, analyzed and visualized data, contributed resources, acquired funding, and contributed to writing the original draft and revisions. All authors had full access to the data, take responsibility for its integrity, and approved the final manuscript.

545 **FIGURE LEGENDS**

546 **Figure 1. Whole-brain axonal projections and largely segregated feedforward and feedback CCPNs**
547 **in VISl. (A)** Top-down views of whole-brain 3D reconstructions of axonal projections from VISl. (Top)
548 L2-4 CCPNs in a *Cux2-IRES-Cre* brain (Experiment: 287495026). (Bottom) L5 CCPNs in a *Tlx3-Cre*
549 brain (Experiment: 520750912). Data adapted from the Allen Brain Connectivity Atlas
550 (https://connectivity.brain-map.org/projection). **(B)** Percentage of total axon projection volume across 13
551 cortical areas from L2-4 VISl CCPNs in *Cux2-IRES-Cre* (magenta, n = 2 mice) and L5 VISl CCPNs in
552 *Tlx3-Cre* (cyan, n = 3 mice). **(C)** Confocal microscope images showing the injection sites of AAVretro-
553 H2B-eGFP, AAVretro-H2B-mCherry, and AAVretro-BFP targeting ACAd/MO, VISp, and VISpm,
554 respectively. Allen Reference Atlas (ARA) section numbers are in the top left corner. **(D)** Representative
555 confocal microscope images showing VISl CCPNs retrogradely labeled based on their axonal projections
556 to ACAd/MO, VISp, or VISpm. Arrows indicate neurons that project to more than one of these target
557 areas. **(E)** Proportions of VISl neurons projecting to multiple target areas. Triple CTB injection
558 experiments show the fraction of VISl neurons projecting to single, double, or all three target areas (ACA,
559 VISp, VISpm). Counts per CCPN type across all animals were: 94 cells for VISl→ACA, 523 cells for
560 VISl→VISp, and 573 cells for VISl→VISpm (n =4 mice). Double CTB injections show the fractions of
561 VISl neurons projecting to one or both target areas (VISp or VISpm). Counts per CCPN type across all
562 animals were: 601 cells for VISl→VISp and 763 cells for VISl→VISpm (n = 3 mice). **(F)** Representative
563 confocal images of CTB-labeled VISl neurons. Top row: Injection sites of CTB tracers conjugated to
564 three fluorophores targeting ACA (yellow), VISp (magenta), and VISpm (cyan); ARA section numbers
565 are indicated above each panel. Middle and bottom rows: VISl CCPNs retrogradely labeled according to
566 their projections. Yellow arrows highlight neurons projecting to ACA, and white arrows indicate neurons
567 projecting to ACA, VISp, and VISpm. **(G)** Percentage distribution of the somata of three VISl CCPN
568 types across cortical layers. A total of 1190 retrograde labeled neurons were analyzed in 6 mice. Data are
569 represented as mean ± SEM.

570 **Figure 2. Long-distance connectivity models and projection- and layer-specific rabies tracing**
571 **strategy. (A)** Three proposed models of long-distance monosynaptic input connectivity to feedforward
572 (FF) and feedback (FB) neurons. **(B)** Schematic of the intersectional rabies tracing strategy for projection-
573 and layer-specific long-distance input tracing to VISl neurons. **(C)** Representative scanning microscope
574 images overlaid with the Allen Brain Common Coordinate Framework reference atlas (Wang et al.,
575 2020), showing AAVretro-tTA targeting in three different areas: VISpm, VISp, and ACA. **(D)**
576 Representative confocal microscope images showing eGFP+mCherry+ starter neurons (arrowheads) in
577 VISl projecting to VISp, VISpm, and ACA in *SepW1-Cre* or *Tlx3-Cre* mice.

578 **Figure 3. Control brains. (A)** Schematic of the viral genetic tracing strategy for control injections
579 without oG (rabies glycoprotein). **(B)** Fluorescence microscope images showing the absence of labeled
580 cells outside the injection sites **(B')**. **(C,E)** Schematic of the viral genetic tracing strategy for control
581 injections without tTA. **(D-D', F-F')** Fluorescence microscope images showing the absence of labeled
582 cells outside the injection sites **(D', F')**. **(G, I)** Schematic of the viral genetic tracing strategy used to
583 verify the axonal projection targets of labeled starter neurons (TVA^{66T}eGFP-P2A-oG+) by CTB
584 injections into either the expected projection target, VISp **(G-H)**, or a non-target area, VISpm **(I-J)**. **(H)**
585 Yellow arrowheads indicate starter neurons co-labeled with eGFP (cyan) and CTB (magenta), indicating
586 their axonal projections to VISp.

587 **Figure 4. Long-distance input mapping of layer- and projection-specific CCPNs in VISl. (A)**
588 Representative confocal images showing long-distance mCherry+ input neurons in LP, VISp, VISpm, and
589 RSP for four distinct feedforward and feedback CCPN types in VISl of *SepW1-Cre* or *Tlx3-Cre* mice. **(B)**
590 The ipsilateral cortical proportion of input neurons across 20 cortical areas, sorted by cortical hierarchy
591 (Harris et al., 2019). The red arrowhead indicates the rank of VISl along the cortical hierarchy. n = 3 mice
592 per each group. Two-way ANOVA with Tukey's multiple comparisons test, * $p<0.05$, ** $p<0.01$, ***
593 $p<0.001$, **** $p<0.0001$. **(C)** Results of one-way ANOVA with Fisher's Least Significant Difference

594 (LSD) post-hoc test for eight selected input regions. *(black) $p<0.05$, *(magenta) $p<0.01$. Data are
595 represented as mean ± SEM.

596 **Figure 5. Further analyses of long-distance input neurons to CCPNs in VISl. (A)** The distributions of
597 presynaptic input neurons across VISp layers to four distinct types of CCPNs in VISl. **(B)** The
598 distribution of presynaptic input neurons across VISpm layers to four distinct types of CCPNs in VISl.
599 **(C)** The proportion of long-distance input neurons located in each of the 20 cortical regions for the three
600 L5 CCPN types in VISl. n = 3 mice per each group for each figure. Two-way ANOVA with Tukey's
601 multiple comparisons test, * $p<0.05$, ** $p<0.01$, **** $p<0.0001$. Data are represented as mean ± SEM.

602 **Figure 6. Long-distance thalamic input mapping of layer- and projection-specific CCPNs in VISl.**
603 **(A)** Representative confocal microscope images showing rabies-labeled mCherry+ input neurons in LGd
604 or LP. **(B)** Proportions of long-distance inputs from each visual thalamic region to four distinct types of
605 feedforward and feedback starter neurons in VISl. n = 3 mice per each group. Two-way ANOVA with
606 Tukey's multiple comparisons test, * $p<0.05$. Data are represented as mean ± SEM.

607 **Table 1. Animal and experimental condition summary**

608 **Table 2. Quantification of rabies tracing in individual mouse brains**

609 **Abbreviations**: AAV, Adeno associated virus; ACA, Anterior cingulate area; ACAd, Anterior cingulate
610 area dorsal; ACAv, Anterior cingulate area ventral; Alp, Agranular insular area, posterior part; AUDd,
611 Dorsal auditory area; AUDp, Primary auditory area; AUDpo, Posterior auditory area; AUDv, Ventral
612 auditory area; CCPN, Cortico-cortical projection neurons; CTB, Cholera toxin subunit B; cTRIO, Cell
613 specific tracing the relationship between input and output; ECT, Ectorhinal area; ENTl, Entorhinal area,
614 lateral part; ENTm, Entorhinal area, medial part, dorsal zone; EnvA, Envelope protein of avian leukosis
615 virus; FB, feedback neurons; FF, feedforward neurons; GU, Gustatory areas; HVA, Higher visual area;
616 LD, Lateral dorsal nucleus of thalamus; LGd, Lateral geniculate nucleus dorsal; LP, Lateral posterior
617 nucleus of the thalamus; Mop, Primary motor area; Mos, Secondary motor cortex; oG, optimized rabies
618 glycoprotein; ORBl, Orbital area, lateral part; PBS, Phosphate buffered saline; PERI, Perirhinal area;
619 PFA, paraformaldehyde; RSP, Retrosplenial cortex; RSPagl, Retrosplenial cortex agranular; RSPd,
620 Retrosplenial cortex dorsal; RSPv, Retrosplenial cortex ventral; SSp-bfd, Primary somatosensory area,
621 barrel field; SSp-ll, Primary somatosensory area, lower limb; SSp-m, Primary somatosensory area,
622 mouth; SSp-n, Primary somatosensory area, nose; SSp-ul, Primary somatosensory area, upper limb; SSp-
623 un, Primary somatosensory area, unassigned; SSp-tr, Primary somatosensory area, trunk; SSs,
624 Supplemental somatosensory area; TEa, Temporal association area; tTa, Tetracycline trans activator;
625 TVA, Receptor for avian leukosis virus; VISa, Anterior area secondary visual cortex; VISal,
626 Anterolateral secondary visual cortex; VISam, Anteromedial secondary visual cortex; VISC, Visceral
627 area; VISl (LM), Lateral secondary visual cortex; VISli, Latero intermediate secondary visual cortex;
628 VISp, Primary visual cortex; VISpl, Posterolateral secondary visual cortex; VISpm, Posteromedial
629 secondary visual cortex; VISpor, Postrhinal secondary visual cortex; VISrl, Rostrolateral secondary visual
630 cortex.

631

632 **REFERENCES**

633 Berezovskii VK, Nassi JJ, Born RT. 2011. Segregation of feedforward and feedback projections in mouse
634 visual cortex. J Comp Neurol [Internet] 519:3672–3683. Available from:
635 http://dx.doi.org/10.1002/cne.22675

636 Bienkowski MS, Benavidez NL, Wu K, Gou L, Becerra M, Dong H-W. 2019. Extrastriate connectivity of
637 the mouse dorsal lateral geniculate thalamic nucleus. J Comp Neurol [Internet] 527:1419–1442.
638 Available from: http://dx.doi.org/10.1002/cne.24627

639 Cajal SR y. 1995. Cajal's histology of the nervous system of man and vertebrates. New York, NY:
640 Oxford University Press.

641 Callaway EM, Luo L. 2015. Monosynaptic circuit tracing with glycoprotein-deleted rabies viruses. J
642 Neurosci [Internet] 35:8979–8985. Available from: http://dx.doi.org/10.1523/JNEUROSCI.0409-
643 15.2015

644 Chatterjee S, Sullivan HA, MacLennan BJ, Xu R, Hou Y, Lavin TK, Lea NE, Michalski JE, Babcock KR,
645 Dietrich S, Matthews GA, Beyeler A, Calhoon GG, Glober G, Whitesell JD, Yao S, Cetin A, Harris
646 JA, Zeng H, Tye KM, Reid RC, Wickersham IR. 2018. Nontoxic, double-deletion-mutant rabies
647 viral vectors for retrograde targeting of projection neurons. Nat Neurosci [Internet] 21:638–646.
648 Available from: https://doi.org/10.1038/s41593-018-0091-7

649 Condylis C, Ghanbari A, Manjrekar N, Bistrong K, Yao S, Yao Z, Nguyen TN, Zeng H, Tasic B, Chen
650 JL. 2022. Dense functional and molecular readout of a circuit hub in sensory cortex. Science
651 [Internet] 375:eabl5981. Available from: http://dx.doi.org/10.1126/science.abl5981

652 Debes SR, Dragoi V. 2023. Suppressing feedback signals to visual cortex abolishes attentional
653 modulation. Science [Internet] 379:468–473. Available from:
654 http://dx.doi.org/10.1126/science.ade1855

655 DeNardo LA, Berns DS, DeLoach K, Luo L. 2015. Connectivity of mouse somatosensory and prefrontal
656 cortex examined with trans-synaptic tracing. Nat Neurosci [Internet] 18:1687–1697. Available from:
657 https://www.nature.com/articles/nn.4131

658 D'Souza RD, Wang Q, Ji W, Meier AM, Kennedy H, Knoblauch K, Burkhalter A. 2022. Hierarchical and
659 nonhierarchical features of the mouse visual cortical network. Nat Commun [Internet] 13:503.
660 Available from: http://dx.doi.org/10.1038/s41467-022-28035-y

661 Felleman DJ, Van Essen DC. 1991. Distributed hierarchical processing in the primate cerebral cortex.
662 Cereb Cortex [Internet] 1:1–47. Available from: http://dx.doi.org/10.1093/cercor/1.1.1-a

663 Fişek M, Herrmann D, Egea-Weiss A, Cloves M, Bauer L, Lee T-Y, Russell LE, Häusser M. 2023.
664 Cortico-cortical feedback engages active dendrites in visual cortex. Nature [Internet] 617:769–776.
665 Available from: http://dx.doi.org/10.1038/s41586-023-06007-6

666 Gămănuţ R, Kennedy H, Toroczkai Z, Ercsey-Ravasz M, Van Essen DC, Knoblauch K, Burkhalter A.
667 2018. The mouse cortical connectome, characterized by an ultra-dense cortical graph, maintains
668 specificity by distinct connectivity profiles. Neuron [Internet] 97:698–715.e10. Available from:
669 http://dx.doi.org/10.1016/j.neuron.2017.12.037

670 Gerfen CR, Paletzki R, Heintz N. 2013. GENSAT BAC cre-recombinase driver lines to study the
671 functional organization of cerebral cortical and basal ganglia circuits. Neuron [Internet] 80:1368–
672 1383. Available from: http://dx.doi.org/10.1016/j.neuron.2013.10.016

673 Han Y, Kebschull JM, Campbell RAA, Cowan D, Imhof F, Zador AM, Mrsic-Flogel TD. 2018. The logic
674 of single-cell projections from visual cortex. Nature [Internet] 556:51–56. Available from:
675 https://pubmed.ncbi.nlm.nih.gov/29590093/

676 Harris JA, Mihalas S, Hirokawa KE, Whitesell JD, Choi H, Bernard A, Bohn P, Caldejon S, Casal L, Cho
677 A, Feiner A, Feng D, Gaudreault N, Gerfen CR, Graddis N, Groblewski PA, Henry AM, Ho A,
678 Howard R, Knox JE, Kuan L, Kuang X, Lecoq J, Lesnar P, Li Y, Luviano J, McConoughey S,
679 Mortrud MT, Naeemi M, Ng L, Oh SW, Ouellette B, Shen E, Sorensen SA, Wakeman W, Wang Q,
680 Wang Y, Williford A, Phillips JW, Jones AR, Koch C, Zeng H. 2019. Hierarchical organization of
681 cortical and thalamic connectivity. Nature [Internet] 575:195–202. Available from:
682 http://dx.doi.org/10.1038/s41586-019-1716-z

683 Harris KD, Shepherd GMG. 2015. The neocortical circuit: themes and variations. Nat Neurosci [Internet]
684 18:170–181. Available from: http://dx.doi.org/10.1038/nn.3917

685 Hupé JM, James AC, Payne BR, Lomber SG, Girard P, Bullier J. 1998. Cortical feedback improves
686 discrimination between figure and background by V1, V2 and V3 neurons. Nature [Internet]
687 394:784–787. Available from: http://dx.doi.org/10.1038/29537

688 Inácio AR, Lam KC, Zhao Y, Pereira F, Gerfen CR, Lee S. 2025. Brain-wide presynaptic networks of
689 functionally distinct cortical neurons. Nature [Internet]:1–11. Available from:
690 https://www.nature.com/articles/s41586-025-08631-w

691 Keller AJ, Roth MM, Scanziani M. 2020. Feedback generates a second receptive field in neurons of the
692 visual cortex. Nature [Internet] 582:545–549. Available from: http://dx.doi.org/10.1038/s41586-020-
693 2319-4

694 Kim EJ, Jacobs MW, Ito-Cole T, Callaway EM. 2016. Improved monosynaptic neural circuit tracing
695 using engineered rabies virus glycoproteins. Cell Rep [Internet] 15:692–699. Available from:
696 http://dx.doi.org/10.1016/j.celrep.2016.03.067

697 Kim EJ, Juavinett AL, Kyubwa EM, Jacobs MW, Callaway EM. 2015. Three types of cortical layer 5
698 neurons that differ in brain-wide connectivity and function. Neuron [Internet] 88:1253–1267.
699 Available from: http://dx.doi.org/10.1016/j.neuron.2015.11.002

700 Kim EJ, Zhang Z, Huang L, Ito-Cole T, Jacobs MW, Juavinett AL, Senturk G, Hu M, Ku M, Ecker JR,
701 Callaway EM. 2020. Extraction of Distinct Neuronal Cell Types from within a Genetically
702 Continuous Population. Neuron [Internet] 107:274–282.e6. Available from:
703 http://dx.doi.org/10.1016/j.neuron.2020.04.018

704 Lavin TK, Jin L, Lea NE, Wickersham IR. 2020. Monosynaptic tracing success depends critically on
705 helper virus concentrations. Front Synaptic Neurosci [Internet] 12:6. Available from:
706 http://dx.doi.org/10.3389/fnsyn.2020.00006

707 Matho KS, Huilgol D, Galbavy W, He M, Kim G, An X, Lu J, Wu P, Di Bella DJ, Shetty AS,
708 Palaniswamy R, Hatfield J, Raudales R, Narasimhan A, Gamache E, Levine JM, Tucciarone J,
709 Szelenyi E, Harris JA, Mitra PP, Osten P, Arlotta P, Huang ZJ. 2021. Genetic dissection of the
710 glutamatergic neuron system in cerebral cortex. Nature [Internet] 598:182–187. Available from:
711 http://dx.doi.org/10.1038/s41586-021-03955-9

712 Miyamichi K, Shlomai-Fuchs Y, Shu M, Weissbourd BC, Luo L, Mizrahi A. 2013. Dissecting local
713 circuits: parvalbumin interneurons underlie broad feedback control of olfactory bulb output. Neuron
714 [Internet] 80:1232–1245. Available from: http://dx.doi.org/10.1016/j.neuron.2013.08.027

715 Nassi JJ, Lomber SG, Born RT. 2013. Corticocortical feedback contributes to surround suppression in V1
716 of the alert primate. J Neurosci [Internet] 33:8504–8517. Available from:
717 http://dx.doi.org/10.1523/JNEUROSCI.5124-12.2013

718 Oh SW, Harris JA, Ng L, Winslow B, Cain N, Mihalas S, Wang Q, Lau C, Kuan L, Henry AM, Mortrud
719 MT, Ouellette B, Nguyen TN, Sorensen SA, Slaughterbeck CR, Wakeman W, Li Y, Feng D, Ho A,
720 Nicholas E, Hirokawa KE, Bohn P, Joines KM, Peng H, Hawrylycz MJ, Phillips JW, Hohmann JG,
721 Wohnoutka P, Gerfen CR, Koch C, Bernard A, Dang C, Jones AR, Zeng H. 2014. A mesoscale
722 connectome of the mouse brain. Nature [Internet] 508:207–214. Available from:
723 http://dx.doi.org/10.1038/nature13186

724 Peng H, Xie P, Liu L, Kuang X, Wang Y, Qu L, Gong H, Jiang S, Li A, Ruan Z, Ding L, Yao Z, Chen C,
725 Chen M, Daigle TL, Dalley R, Ding Z, Duan Y, Feiner A, He P, Hill C, Hirokawa KE, Hong G,
726 Huang L, Kebede S, Kuo H-C, Larsen R, Lesnar P, Li L, Li Q, Li X, Li Y, Li Y, Liu A, Lu D, Mok
727 S, Ng L, Nguyen TN, Ouyang Q, Pan J, Shen E, Song Y, Sunkin SM, Tasic B, Veldman MB,
728 Wakeman W, Wan W, Wang P, Wang Q, Wang T, Wang Y, Xiong F, Xiong W, Xu W, Ye M, Yin
729 L, Yu Y, Yuan J, Yuan J, Yun Z, Zeng S, Zhang S, Zhao S, Zhao Z, Zhou Z, Huang ZJ, Esposito L,
730 Hawrylycz MJ, Sorensen SA, Yang XW, Zheng Y, Gu Z, Xie W, Koch C, Luo Q, Harris JA, Wang
731 Y, Zeng H. 2021. Morphological diversity of single neurons in molecularly defined cell types.
732 Nature [Internet] 598:174–181. Available from: https://doi.org/10.1038/s41586-021-03941-1

733 Ren J, Friedmann D, Xiong J, Liu CD, Ferguson BR, Weerakkody T, DeLoach KE, Ran C, Pun A, Sun
734 Y, Weissbourd B, Neve RL, Huguenard J, Horowitz MA, Luo L. 2018. Anatomically defined and
735 functionally distinct dorsal raphe serotonin sub-systems. Cell [Internet] 175:472–487.e20. Available
736 from: http://dx.doi.org/10.1016/j.cell.2018.07.043

737 Schwarz LA, Miyamichi K, Gao XJ, Beier KT, Weissbourd B, DeLoach KE, Ren J, Ibanes S, Malenka
738 RC, Kremer EJ, Luo L. 2015. Viral-genetic tracing of the input-output organization of a central
739 noradrenaline circuit. Nature [Internet] 524:88–92. Available from:
740 https://www.nature.com/articles/nature14600

741 Siegle JH, Jia X, Durand S, Gale S, Bennett C, Graddis N, Heller G, Ramirez TK, Choi H, Luviano JA,
742 Groblewski PA, Ahmed R, Arkhipov A, Bernard A, Billeh YN, Brown D, Buice MA, Cain N,
743 Caldejon S, Casal L, Cho A, Chvilicek M, Cox TC, Dai K, Denman DJ, de Vries SEJ, Dietzman R,
744 Esposito L, Farrell C, Feng D, Galbraith J, Garrett M, Gelfand EC, Hancock N, Harris JA, Howard
745 R, Hu B, Hytnen R, Iyer R, Jessett E, Johnson K, Kato I, Kiggins J, Lambert S, Lecoq J,
746 Ledochowitsch P, Lee JH, Leon A, Li Y, Liang E, Long F, Mace K, Melchior J, Millman D,
747 Mollenkopf T, Nayan C, Ng L, Ngo K, Nguyen T, Nicovich PR, North K, Ocker GK, Ollerenshaw
748 D, Oliver M, Pachitariu M, Perkins J, Reding M, Reid D, Robertson M, Ronellenfitch K, Seid S,
749 Slaughterbeck C, Stoecklin M, Sullivan D, Sutton B, Swapp J, Thompson C, Turner K, Wakeman
750 W, Whitesell JD, Williams D, Williford A, Young R, Zeng H, Naylor S, Phillips JW, Reid RC,
751 Mihalas S, Olsen SR, Koch C. 2021. Survey of spiking in the mouse visual system reveals functional
752 hierarchy. Nature [Internet] 592:86–92. Available from: http://dx.doi.org/10.1038/s41586-020-
753 03171-x

754 Siu C, Balsor J, Merlin S, Federer F, Angelucci A. 2021. A direct interareal feedback-to-feedforward
755 circuit in primate visual cortex. Nat Commun [Internet] 12:4911. Available from:
756 http://dx.doi.org/10.1038/s41467-021-24928-6

757 Soronow ALR, Jacobs MW, Dickson RG, Kim EJ. 2025. Bell Jar: A semiautomated registration and cell
758 counting tool for mouse neurohistology analysis. eNeuro [Internet] 12. Available from:
759 http://dx.doi.org/10.1523/ENEURO.0036-23.2025

Experiment	Mouse ID	Sex	Strain	From	Projection	Mouse age (P) at virus #1/#2 injection	Virus #1a (oG) and #1b (TVA)	Virus #1a (oG) titer	Virus #1b (TVA) titer	Virus #2 AAVretro	Virus #2 titer	Mouse age (P) at virus #3 injection	Virus #3 (rabies)	Virus #3 titer	Total virus/tracer incubation time (day)
FF/FB identity: Triple AAV	414	F	C57	VISl	ACA, VISp, VISpm	89	50 nl of scAAVretro-hSyn-H2B-eGFP into ACA, 50 nl of scAAVretro-hSyn-H2B-mCherry into VISp, 50 nl of AAVretro-BFP into VISpm	NA	NA	NA	NA	NA	NA	NA	21
FF/FB identity: Triple AAV	415	F	C57	VISl	ACA, VISp, VISpm	89	50 nl of scAAVretro-hSyn-H2B-eGFP into VISp, 50 nl of scAAVretro-hSyn-H2B-mCherry into VISpm, 50 nl of AAVretro-BFP into ACA	NA	NA	NA	NA	NA	NA	NA	21
FF/FB Identity: Double CTB	124	F	Tlx3-Cre	VISl	VISpm, VISp	104	50 nl of CTB-555 in VISpm, 50 nl of CTB-647 in VISp	NA	NA	NA	NA	NA	NA	NA	3
FF/FB Identity: Triple CTB	353	M	SepW1-Cre	VISl	ACA, VISp, VISpm	72	50 nl of CTB-647 in VISpm, 50 nl of CTB-555 in VISp, 50 nl of CTB-488 in ACA	NA	NA	NA	NA	NA	NA	NA	4
FF/FB Identity: Triple CTB	354	M	SepW1-Cre	VISl	ACA, VISp, VISpm	72	50 nl of CTB-555 in VISpm, 50 nl of CTB-488 in VISp, 50 nl of CTB-647 in ACA	NA	NA	NA	NA	NA	NA	NA	4
FF/FB Identity: Triple CTB	JR0845	M	C57	VISl	ACA, VISp, VISpm	64	50 nl of CTB-555 in VISpm, 50 nl of CTB-488 in VISp, 50 nl of CTB-647 in ACA	NA	NA	NA	NA	NA	NA	NA	6
FF/FB Identity: Triple CTB	JR0846	M	C57	VISl	ACA, VISp, VISpm	61	50 nl of CTB-647 in VISpm, 50 nl of CTB-555 in VISp, 50 nl of CTB-488 in ACA	NA	NA	NA	NA	NA	NA	NA	6
FF/FB Identity: Triple CTB	JR0847	M	C57	VISl	ACA, VISp, VISpm	61	50 nl of CTB-488 in VISpm, 50 nl of CTB-647 in VISp, 50 nl of CTB-555 in ACA	NA	NA	NA	NA	NA	NA	NA	6
FF/FB Identity: Triple CTB	JR0848	M	C57	VISl	ACA, VISp, VISpm	61	50 nl of CTB-555 in VISpm, 50 nl of CTB-488 in VISp, 50 nl of CTB-647 in ACA	NA	NA	NA	NA	NA	NA	NA	6
FF/FB Identity: Triple CTB	JR0849	M	C57	VISl	ACA, VISp, VISpm	61	50 nl of CTB-647 in VISpm, 50 nl of CTB-555 in VISp, 50 nl of CTB-488 in ACA	NA	NA	NA	NA	NA	NA	NA	6
FF/FB Identity: Triple CTB	JR0850	M	C57	VISl	ACA, VISp, VISpm	61	50 nl of CTB-488 in VISpm, 50 nl of CTB-647 in VISp, 50 nl of CTB-555 in ACA	NA	NA	NA	NA	NA	NA	NA	6
Control: No G-protein test	392	M	Tlx3-Cre	VISl	VISp	91	50 nl mixture of PBS and AAV8-TRE-DIO-eGFP-T2A-TVA into VISl	NA	7.00E+12	50 nl of AAVretro-nEF-lox66/71-tTA	4.86E+13	105	100 nl of EnvA+RVdG-mCherry into VISl	1.43E+10	21
Control: No G-protein test	406	M	Tlx3-Cre	VISl	VISp	139	50 nl mixture of PBS and AAV8-TRE-DIO-eGFP-T2A-TVA into VISl	NA	7.00E+12	50 nl of AAVretro-nEF-lox66/71-tTA	4.86E+13	153	100 nl of EnvA+RVdG-mCherry into VISl	1.43E+10	21
Control: No G-protein test	405	M	Tlx3-Cre	VISl	VISp	139	50 nl mixture of PBS and AAV8-TRE-DIO-eGFP-T2A-TVA into VISl	NA	7.00E+12	50 nl of AAVretro-nEF-lox66/71-tTA	4.86E+13	153	100 nl of EnvA+RVdG-mCherry into VISl	1.43E+10	21
Control: Colocalization AAV retro with CTB	386	F	Tlx3-Cre	VISl	VISp	126	50 nl of AAV8-TRE-DIO-TVA66TeGFP-P2A-oG into VISl. 50 nl of CTB-647 in VISpm, 50 nl of CTB-555 in VISp	7.44E+13	NA	50 nl of AAVretro-nEF-lox66/71-tTA	4.86E+13	126	NA	NA	14
Control: Colocalization AAV retro with CTB	403	F	SepW1-Cre	VISl	VISp	131	50 nl of AAV8-TRE-DIO-TVA66TeGFP-P2A-oG into VISl. 50 nl of CTB-647 in VISp, 50 nl of CTB-555 in VISpm	7.44E+13	NA	50 nl of AAVretro-nEF-lox66/71-tTA	4.86E+13	NA	NA	NA	14
Control: Colocalization AAV retro with CTB	343	F	Tlx3-Cre	VISl	VISpm	149	50 nl mixture of AAV8-TRE-DIO-oG and AAV8-TRE-DIO-GFP-T2A-TVA into VISl. 10 nl of CTB-647 into VISpm	2.36E+13	7.00E+12	50 nl of AAVretro-nEF-lox66/71-tTA	4.86E+13	163	100 nl of EnvA+RVdG-mCherry into VISl	7.71E+08	21
Control: Colocalization AAV retro with CTB	344	F	Tlx3-Cre	VISl	VISpm	140	50 nl mixture of AAV8-TRE-DIO-oG and AAV8-TRE-DIO-GFP-T2A-TVA into VISl. 10 nl of CTB-647 into VISpm	2.36E+13	7.00E+12	50 nl of AAVretro-nEF-lox66/71-tTA	4.86E+13	154	100 nl of EnvA+RVdG-mCherry into VISl	7.71E+08	21
Control: No TTA test	94	M	Tlx3-Cre	VISl	NA	337	50 nl of AAV8-TRE-DIO-TVA66TeGFP-P2A-oG into VISl	7.44E+13	NA	NA	NA	NA	NA	NA	21
Control: No TTA test	425	M	SepW1-Cre	VISl	NA	74	50 nl of AAV8-TRE-DIO-TVA66TeGFP-P2A-oG into VISl	7.44E+13	7.44E+13	NA	NA	84	100 nl of EnvA+RVdG-mCherry into VISl	7.11E+09	21
Control: No TTA test	427	F	SepW1-Cre	VISl/VISp	NA	63	50 nl mixture of AAV8-TRE-DIO-oG and AAV8-TRE-DIO-GFP-T2A-TVA	1.41E+14	7.00E+12	NA	NA	77	100 nl of EnvA+RVdG-mCherry into VISl	7.11E+09	21
Control: No TTA test	428	F	SepW1-Cre	VISl/VISp	NA	63	50 nl mixture of AAV8-TRE-DIO-oG and AAV8-TRE-DIO-GFP-T2A-TVA	1.41E+14	7.00E+12	NA	NA	77	100 nl of EnvA+RVdG-mCherry into VISl	7.11E+09	21
Control: No TTA test	429	F	Tlx3-Cre	VISl	NA	51	50 nl of AAV8-TRE-DIO-TVA66TeGFP-P2A-oG into VISl	7.44E+13	7.44E+13	NA	NA	65	100 nl of EnvA+RVdG-mCherry into VISl	7.11E+09	21
Control: No TTA test	432	F	Tlx3-Cre	VISl	NA	49	50 nl of AAV8-TRE-DIO-TVA66TeGFP-P2A-oG into VISl	7.44E+13	7.44E+13	NA	NA	63	100 nl of EnvA+RVdG-mCherry into VISl	7.11E+09	21
Rabies: L2/3 VISl-VISpm	326	M	SepW1-Cre	VISl	VISpm	73	50 nl mixture of AAV8-TRE-DIO-oG and AAV8-TRE-DIO-GFP-T2A-TVA into VISl	2.36E+13	7.00E+12	50 nl of AAVretro-nEF-lox66/71-tTA	4.86E+13	87	100 nl of EnvA+RVdG-mCherry into VISl	7.71E+08	21
Rabies: L2/3 VISl-VISpm	327	M	SepW1-Cre	VISl	VISpm	73	50 nl mixture of AAV8-TRE-DIO-oG and AAV8-TRE-DIO-GFP-T2A-TVA into VISl	2.36E+13	7.00E+12	50 nl of AAVretro-nEF-lox66/71-tTA	4.86E+13	87	100 nl of EnvA+RVdG-mCherry into VISl	7.71E+08	21
Rabies: L2/3 VISl-VISpm	328	M	SepW1-Cre	VISl	VISpm	73	50 nl mixture of AAV8-TRE-DIO-oG and AAV8-TRE-DIO-GFP-T2A-TVA into VISl	2.36E+13	7.00E+12	50 nl of AAVretro-nEF-lox66/71-tTA	4.86E+13	87	100 nl of EnvA+RVdG-mCherry into VISl	7.71E+08	21
Rabies: L2/3 VISl-VISp	329	M	SepW1-Cre	VISl	VISp	68	50 nl mixture of AAV8-TRE-DIO-oG and AAV8-TRE-DIO-GFP-T2A-TVA into VISl	2.36E+13	7.00E+12	50 nl of AAVretro-nEF-lox66/71-tTA	4.86E+13	82	100 nl of EnvA+RVdG-mCherry into VISl	7.71E+08	21
Rabies: L2/3 VISl-VISp	161	F	SepW1-Cre	VISl	VISp	67	50 nl mixture of AAV8-TRE-DIO-oG and AAV8-TRE-DIO-GFP-T2A-TVA	1.41E+14	7.00E+12	50 nl of AAVretro-nEF-lox66/71-tTA	4.86E+13	81	100 nl of EnvA+RVdG-mCherry into VISl	7.71E+08	21
Rabies: L2/3 VISl-VISp	60	F	SepW1-Cre	VISl	VISp	65	50 nl of AAV8-TRE-DIO-TVA66TeGFP-P2A-oG into VISl	7.44E+13	NA	100 nl of AAVretro-nEF-lox66/71-tTA	4.86E+13	79	100 nl of EnvA+RVdG-mCherry into VISl	1.78E+09	21
Rabies: L5 VISl-VISpm	67	F	Tlx3-Cre	VISl	VISpm	69	50 nl of AAV8-TRE-DIO-TVA66TeGFP-P2A-oG into VISl	7.44E+13	NA	50 nl of AAVretro-nEF-lox66/71-tTA	4.86E+13	83	100 nl of EnvA+RVdG-mCherry into VISl	1.07E+09	21
Rabies: L5 VISl-VISpm	143	M	Tlx3-Cre	VISl	VISpm	65	50 nl mixture of AAV8-TRE-DIO-oG and AAV8-TRE-DIO-GFP-T2A-TVA into VISl	1.41E+14	7.00E+12	50 nl of AAVretro-nEF-lox66/71-tTA	4.86E+13	79	100 nl of EnvA+RVdG-mCherry into VISl	7.71E+08	21
Rabies: L5 VISl-VISpm	118	F	Tlx3-Cre	VISl	VISpm	106	50 nl mixture of AAV8-TRE-DIO-oG and AAV8-TRE-DIO-GFP-T2A-TVA into VISl	1.41E+14	7.00E+12	50 nl of AAVretro-nEF-lox66/71-tTA	4.86E+13	120	100 nl of EnvA+RVdG-mCherry into VISl	1.07E+09	21
Rabies: L5 VISl-ACA	325	M	Tlx3-Cre	VISl	ACA	92	50 nl mixture of AAV8-TRE-DIO-oG and AAV8-TRE-DIO-GFP-T2A-TVA into VISl	2.36E+13	7.00E+12	50 nl of AAVretro-nEF-lox66/71-tTA	4.86E+13	106	100 nl of EnvA+RVdG-mCherry into VISl	7.71E+08	21
Rabies: L5 VISl-ACA	356	F	Tlx3-Cre	VISl	ACA	74	50 nl mixture of AAV8-TRE-DIO-oG and AAV8-TRE-DIO-GFP-T2A-TVA into VISl	2.36E+13	7.00E+12	50 nl of AAVretro-nEF-lox66/71-tTA	4.86E+13	89	100 nl of EnvA+RVdG-mCherry into VISl	7.71E+08	21
Rabies: L5 VISl-ACA	396	F	Tlx3-Cre	VISl	ACA	125	50 nl mixture of AAV8-TRE-DIO-oG and AAV8-TRE-DIO-GFP-T2A-TVA into VISl	1.41E+14	7.00E+12	50 nl of AAVretro-nEF-lox66/71-tTA	4.86E+13	139	100 nl of EnvA+RVdG-mCherry into VISl	1.43E+10	21
Rabies: L5 VISl-VISp	122	F	Tlx3-Cre	VISl	VISp	97	50 nl mixture of AAV8-TRE-DIO-oG and AAV8-TRE-DIO-GFP-T2A-TVA into VISl	1.41E+14	7.00E+12	50 nl of AAVretro-nEF-lox66/71-tTA	4.86E+13	111	100 nl of EnvA+RVdG-mCherry into VISl	1.07E+09	21
Rabies: L5 VISl-VISp	63	M	Tlx3-Cre	VISl	VISp	70	50 nl of AAV8-TRE-DIO-TVA66TeGFP-P2A-oG into VISl	7.44E+13	NA	200 nl of AAVretro-nEF-lox66/71-tTA	4.86E+13	84	100 nl of EnvA+RVdG-mCherry into VISl	1.78E+09	21
Rabies: L5 VISl-VISp	64	F	Tlx3-Cre	VISl	VISp	71	50 nl of AAV8-TRE-DIO-TVA66TeGFP-P2A-oG into VISl	7.44E+13	NA	100 nl of AAVretro-nEF-lox66/71-tTA	4.86E+13	85	100 nl of EnvA+RVdG-mCherry into VISl	1.07E+09	21

Raw counts in each brain area

Experiment	Mouse ID	VISp	AUDp	SSp-n	AUDv	SSp-ll	AUDd	SSp-un	SSp-ul	SSp-m	SSp-bfd	SSs	VISrl	RSPd	MOp	VISpl	RSPagl	RSPv	VISal	VISpm	SSp-tr	ORBl	AUDpo	VISpor	ACAv	VISam	VISa	ECT	MOs	PERI	TEa	AIp	GU	VISC	ACAd	ENTl	ENTm
L2/3 VISl-VISpm	326	660	129	1	32	12	151	16	13	0	144	103	69	16	11	3	14	5	40	161	102	3	78	31	2	23	183	2	17	0	18	0	2	4	15	18	3
L2/3 VISl-VISpm	327	1038	184	1	21	1	55	4	3	2	98	26	140	50	2	14	30	7	72	128	7	1	64	61	0	42	55	4	17	0	77	2	0	1	7	5	15
L2/3 VISl-VISpm	328	193	15	0	0	0	13	0	0	0	17	6	46	1	0	0	8	5	33	32	1	0	6	3	1	15	4	1	9	2	19	1	0	0	2	1	0
L2/3 VISl-VISp	60	94	23	0	3	0	14	0	0	0	14	2	14	1	0	1	2	0	11	11	1	0	15	4	0	8	12	1	0	0	10	0	0	0	1	6	5
L2/3 VISl-VISp	161	403	54	0	18	0	27	0	1	0	30	11	32	31	0	22	26	14	36	32	2	0	16	27	0	12	15	8	0	1	64	3	0	12	0	22	3
L2/3 VISl-VISp	329	1191	238	0	41	5	161	0	7	0	256	74	307	93	9	31	58	49	19	175	58	9	60	18	2	264	299	3	49	1	36	2	1	1	49	5	11
L5 VISl-VISpm	67	76	0	1	0	1	0	0	0	0	0	5	7	10	0	0	5	5	7	2	0	0	0	2	0	2	0	1	1	1	1	2	0	3	0	10	2
L5 VISl-VISpm	118	290	7	0	2	1	14	1	2	0	18	0	27	29	0	3	45	10	18	21	2	0	3	60	0	27	4	0	0	0	29	2	0	0	0	0	1
L5 VISl-VISpm	143	601	12	0	10	0	10	3	1	0	28	22	42	60	0	16	54	63	61	25	7	0	10	44	0	24	55	0	0	0	86	1	0	3	0	4	4
L5 VISl-VISp	63	226	4	7	8	4	3	0	0	0	13	9	22	20	0	4	10	6	30	14	5	0	1	9	2	6	2	0	0	0	0	2	0	1	2	4	0
L5 VISl-VISp	64	646	32	0	10	0	2	0	0	0	17	4	40	21	0	22	5	10	30	23	3	0	57	29	0	15	7	3	0	1	63	0	0	0	0	2	2
L5 VISl-VISp	122	308	12	1	2	3	2	0	0	0	9	2	34	7	0	32	7	6	22	15	1	0	10	39	0	1	0	0	0	0	10	0	0	1	0	3	0
L5 VISl-ACA	325	320	20	0	0	0	14	0	0	0	24	16	42	34	0	4	41	3	12	25	4	0	2	14	0	12	14	0	0	0	11	0	0	0	0	3	2
L5 VISl-ACA	356	103	7	0	3	0	1	1	0	0	5	1	9	2	0	0	1	0	41	2	0	0	4	2	0	0	0	0	1	0	19	0	0	1	0	0	1
L5 VISl-ACA	396	164	35	0	67	0	18	0	0	0	12	23	21	11	0	0	4	9	0	6	0	0	14	17	0	16	15	38	0	14	79	0	0	0	0	12	5

Proportion of ipsilateral cortical inputs

Experiment	VISp	AUDp	SSp-n	AUDv	SSp-ll	AUDd	SSp-un	SSp-ul	SSp-m	SSp-bfd	SSs	VISrl	RSPd	MOp	VISpl	RSPagl	RSPv	VISal	VISpm	SSp-tr	ORBl	AUDpo	VISpor	ACAv	VISam	VISa	ECT	MOs	PERI	TEa	AIp	GU	VISC	ACAd	ENTl	ENTm
L2/3 VISl-VISpm	31.75%	6.20%	0.05%	1.54%	0.58%	7.26%	0.77%	0.63%	0.00%	6.93%	4.95%	3.32%	0.77%	0.53%	0.14%	0.67%	0.24%	1.92%	7.74%	4.91%	0.14%	3.75%	1.49%	0.10%	1.11%	8.80%	0.08%	0.82%	0.00%	0.87%	0.00%	0.10%	0.19%	0.72%	0.87%	0.14%
L2/3 VISl-VISpm	46.55%	8.25%	0.04%	0.94%	0.04%	2.47%	0.18%	0.13%	0.09%	4.39%	1.17%	6.28%	2.24%	0.09%	0.63%	1.35%	0.31%	3.23%	5.74%	0.31%	0.04%	2.87%	2.74%	0.00%	1.88%	2.47%	0.14%	0.76%	0.00%	3.45%	0.09%	0.00%	0.04%	0.31%	0.22%	0.67%
L2/3 VISl-VISpm	44.57%	3.46%	0.00%	0.00%	0.00%	3.00%	0.00%	0.00%	0.00%	3.93%	1.39%	10.62%	0.23%	0.00%	0.00%	1.85%	1.15%	7.62%	7.39%	0.23%	0.00%	1.39%	0.69%	0.23%	3.46%	0.92%	0.14%	2.08%	0.46%	4.39%	0.23%	0.00%	0.00%	0.46%	0.23%	0.00%
L2/3 VISl-VISp	37.30%	9.13%	0.00%	1.19%	0.00%	5.56%	0.00%	0.00%	0.00%	5.56%	0.79%	5.56%	0.40%	0.00%	0.40%	0.79%	0.00%	4.37%	4.37%	0.40%	0.00%	5.95%	1.59%	0.00%	3.17%	4.76%	0.19%	0.00%	0.00%	3.97%	0.00%	0.00%	0.00%	0.40%	2.38%	1.98%
L2/3 VISl-VISp	44.09%	5.91%	0.00%	1.97%	0.00%	2.95%	0.00%	0.11%	0.00%	3.28%	1.20%	3.50%	3.39%	0.00%	2.41%	2.84%	1.53%	3.94%	3.50%	0.22%	0.00%	1.75%	2.95%	0.00%	1.31%	1.64%	0.43%	0.00%	0.11%	7.00%	0.33%	0.00%	1.31%	0.00%	2.41%	0.33%
L2/3 VISl-VISp	33.28%	6.65%	0.00%	1.15%	0.14%	4.50%	0.00%	0.20%	0.00%	7.15%	2.07%	8.58%	2.60%	0.25%	0.87%	1.62%	1.37%	0.53%	4.89%	1.62%	0.25%	1.68%	0.50%	0.06%	7.38%	8.35%	0.07%	1.37%	0.03%	1.01%	0.06%	0.03%	0.03%	1.37%	0.14%	0.31%
L5 VISl-VISpm	53.52%	0.00%	0.70%	0.00%	0.70%	0.00%	0.00%	0.00%	0.00%	0.00%	3.52%	4.93%	7.04%	0.00%	0.00%	3.52%	3.52%	4.93%	1.41%	0.00%	0.00%	0.00%	1.41%	0.00%	1.41%	0.00%	0.36%	0.70%	0.00%	0.70%	1.41%	0.00%	2.11%	0.00%	7.04%	1.41%
L5 VISl-VISpm	47.08%	1.14%	0.00%	0.32%	0.16%	2.27%	0.16%	0.32%	0.00%	2.92%	0.00%	4.38%	4.71%	0.00%	0.49%	7.31%	1.62%	2.92%	3.41%	0.32%	0.00%	0.49%	9.74%	0.00%	4.38%	0.65%	0.00%	0.00%	0.00%	4.71%	0.32%	0.00%	0.00%	0.00%	0.00%	0.16%
L5 VISl-VISpm	48.23%	0.96%	0.00%	0.80%	0.00%	0.80%	0.24%	0.08%	0.00%	2.25%	1.77%	3.37%	4.82%	0.00%	1.28%	4.33%	5.06%	4.90%	2.01%	0.56%	0.00%	0.80%	3.53%	0.00%	1.93%	4.41%	0.00%	0.00%	0.00%	6.90%	0.08%	0.00%	0.24%	0.00%	0.32%	0.32%
L5 VISl-VISp	54.59%	0.97%	1.69%	1.93%	0.97%	0.72%	0.00%	0.00%	0.00%	3.14%	2.17%	5.31%	4.83%	0.00%	0.97%	2.42%	1.45%	7.25%	3.38%	1.21%	0.00%	0.24%	2.17%	0.48%	1.45%	0.48%	0.00%	0.00%	0.00%	0.00%	0.48%	0.00%	0.24%	0.48%	0.97%	0.00%
L5 VISl-VISp	62.06%	3.07%	0.00%	0.96%	0.00%	0.19%	0.00%	0.00%	0.00%	1.63%	0.38%	3.84%	2.02%	0.00%	2.11%	0.48%	0.96%	2.88%	2.21%	0.29%	0.00%	5.48%	2.79%	0.00%	1.44%	0.67%	0.13%	0.00%	0.10%	6.05%	0.00%	0.00%	0.00%	0.00%	0.19%	0.19%
L5 VISl-VISp	58.44%	2.28%	0.19%	0.38%	0.57%	0.38%	0.00%	0.00%	0.00%	1.71%	0.38%	6.45%	1.33%	0.00%	6.07%	1.33%	1.14%	4.17%	2.85%	0.19%	0.00%	1.90%	7.40%	0.00%	0.19%	0.00%	0.00%	0.00%	0.00%	1.90%	0.00%	0.00%	0.19%	0.00%	0.57%	0.00%
L5 VISl-ACA	51.86%	3.24%	0.00%	0.00%	0.00%	2.27%	0.00%	0.00%	0.00%	3.89%	2.59%	6.81%	5.51%	0.00%	0.65%	6.65%	0.49%	1.94%	4.05%	0.65%	0.00%	0.32%	2.27%	0.00%	1.94%	2.27%	0.00%	0.00%	0.00%	1.78%	0.00%	0.00%	0.00%	0.00%	0.49%	0.32%
L5 VISl-ACA	50.49%	3.43%	0.00%	1.47%	0.00%	0.49%	0.49%	0.00%	0.00%	2.45%	0.49%	4.41%	0.98%	0.00%	0.00%	0.49%	0.00%	20.10%	0.98%	0.00%	0.00%	1.96%	0.98%	0.00%	0.00%	0.00%	0.00%	0.49%	0.00%	9.31%	0.00%	0.00%	0.49%	0.00%	0.00%	0.49%
L5 VISl-ACA	30.26%	6.46%	0.00%	12.36%	0.00%	3.32%	0.00%	0.00%	0.00%	2.21%	4.24%	3.87%	2.03%	0.00%	0.00%	0.74%	1.66%	0.00%	1.11%	0.00%	0.00%	2.58%	3.14%	0.00%	2.95%	2.77%	7.01%	0.00%	2.58%	14.58%	0.00%	0.00%	0.00%	0.00%	2.21%	0.92%

Proportion of thalamic inputs

Experiment	LGd	LD	LP	LGd	LD	LP
L2/3 VISl-VISpm	4	1	41	8.70%	2.17%	89.13%
L2/3 VISl-VISpm	9	1	73	10.84%	1.20%	87.95%
L2/3 VISl-VISpm	1	0	8	11.11%	0.00%	88.89%
L2/3 VISl-VISp	1	0	5	16.67%	0.00%	83.33%
L2/3 VISl-VISp	30	2	58	33.33%	2.22%	64.44%
L2/3 VISl-VISp	17	12	137	10.24%	7.23%	82.53%
L5 VISl-VISpm	3	0	6	33.33%	0.00%	66.67%
L5 VISl-VISpm	23	3	59	27.06%	3.53%	69.41%
L5 VISl-VISpm	46	3	77	36.51%	2.38%	61.11%
L5 VISl-VISp	5	1	21	18.52%	3.70%	77.78%
L5 VISl-VISp	17	3	101	14.05%	2.48%	83.47%
L5 VISl-VISp	13	0	23	36.11%	0.00%	63.89%
L5 VISl-ACA	NA	NA	NA	NA	NA	NA
L5 VISl-ACA	NA	NA	NA	NA	NA	NA
L5 VISl-ACA	NA	NA	NA	NA	NA	NA

Projection- and layer- specific long-range input tracing

SepW1-Cre (L2/3) or Tlx3-Cre (L5 CCPNs)

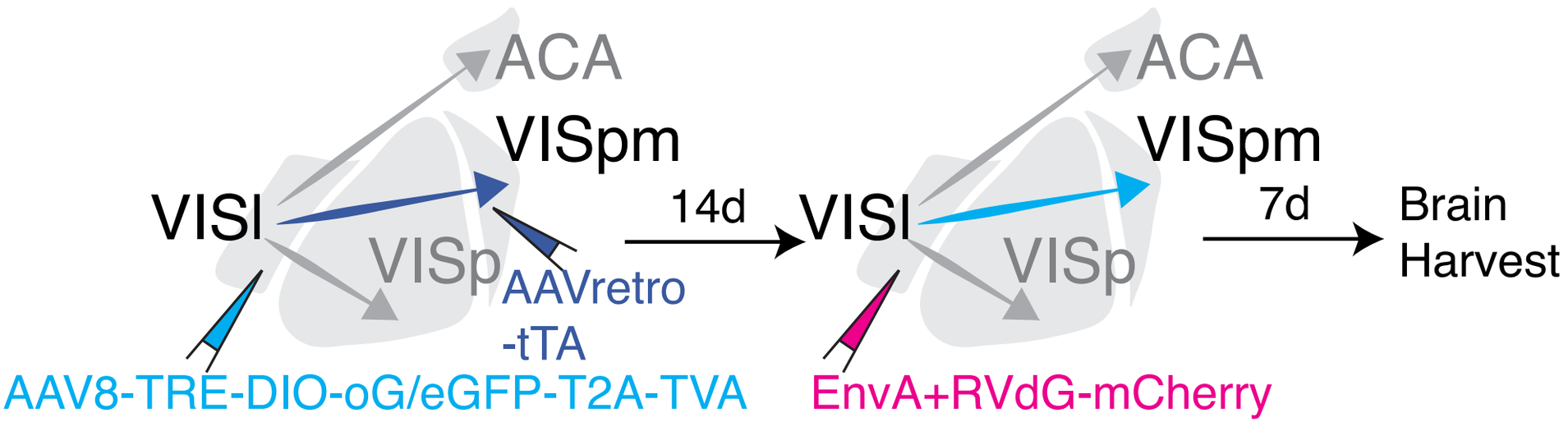

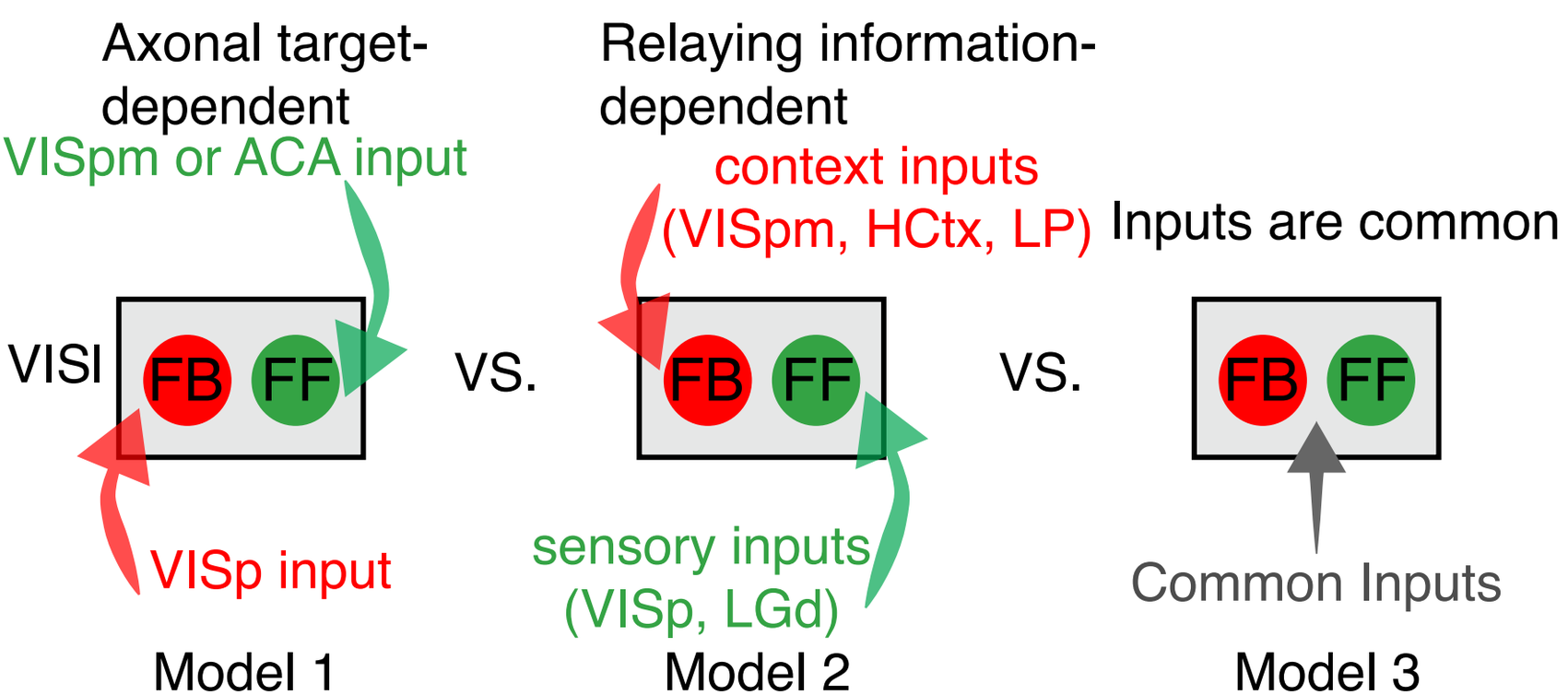

Figure 1

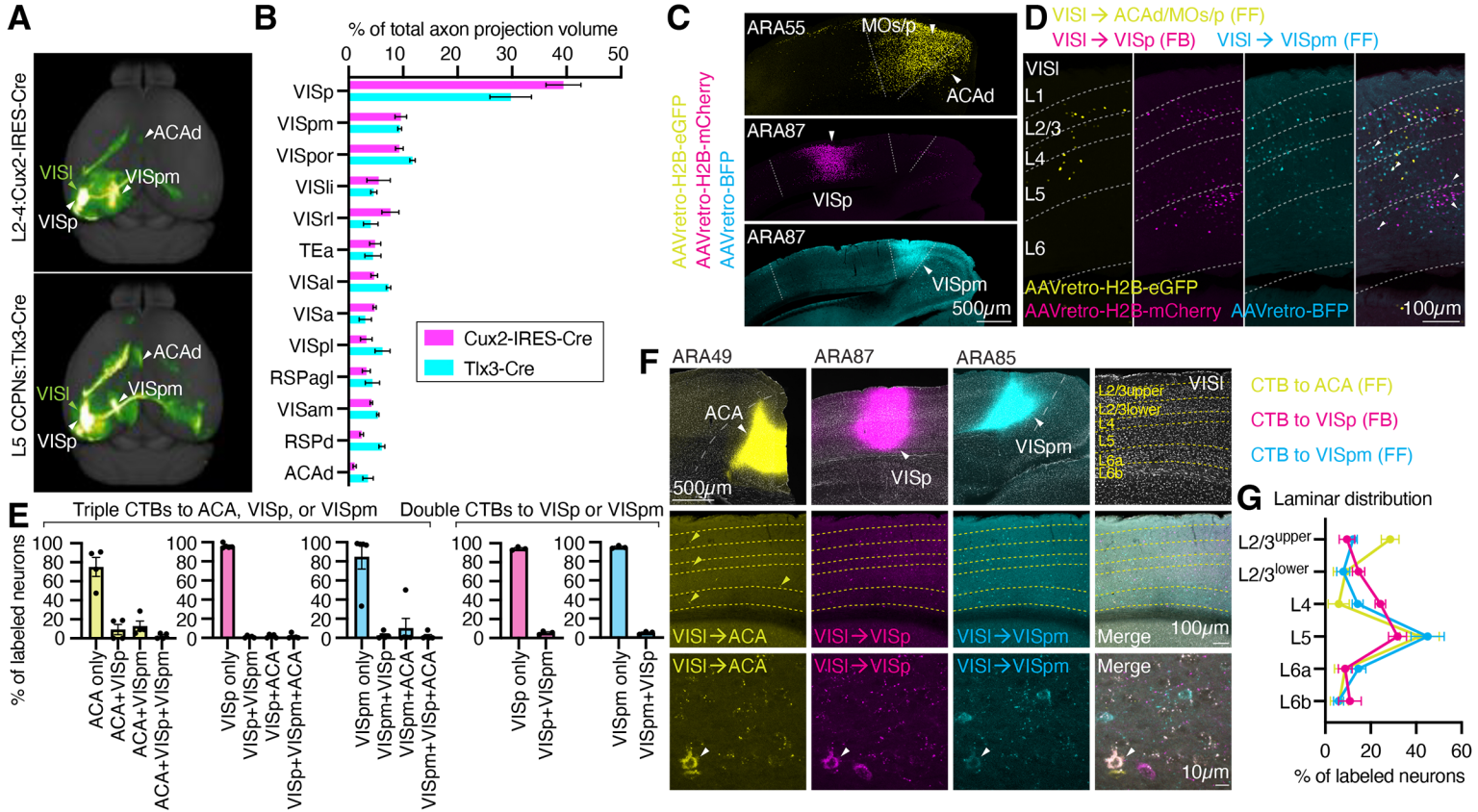
A
L2-4:Cux2-IRES-Cre
ACAd
VISl
VISpm
VISp
L5 CCPNs:Tlx3-Cre
ACAd
VISl
VISpm
VISp
B
% of total axon projection volume
0 10 20 30 40 50
VISp
VISpm
VISpor
VISli
VISrl
TEa
VISal
VISa
VISpl
RSPagl
VISam
RSPd
ACAd
Cux2-IRES-Cre
Tlx3-Cre
C
AAVretro-H2B-eGFP
AAVretro-H2B-mCherry
AAVretro-BFP
ARA55
MOs/p
ACAd
ARA87
VISp
ARA87
VISpm
500μm
D
VISl → ACAd/MOs/p (FF)
VISl → VISp (FB)
VISl → VISpm (FF)
VISl
L1
L2/3
L4
L5
L6
AAVretro-H2B-eGFP
AAVretro-H2B-mCherry
AAVretro-BFP
100μm
E
Triple CTBs to ACA, VISp, or VISpm
Double CTBs to VISp or VISpm
% of labeled neurons
100 80 60 40 20 0
ACA only
ACA+VISp
ACA+VISpm
ACA+VISp+VISpm
VISp only
VISp+VISpm
VISp+ACA
VISp+VISpm+ACA
VISpm only
VISpm+VISp
VISpm+ACA
VISpm+VISp+ACA
VISp only
VISp+VISpm
VISpm only
VISpm+VISp
F
ARA49
ARA87
ARA85
ACA
VISp
VISpm
VISl
L2/3upper
L2/3lower
L4
L5
L6a
L6b
500μm
CTB to ACA (FF)
CTB to VISp (FB)
CTB to VISpm (FF)
VISl→ACA
VISl→VISp
VISl→VISpm
Merge
100μm
10μm
G
Laminar distribution
L2/3upper
L2/3lower
L4
L5
L6a
L6b
0 20 40 60
% of labeled neurons

Figure 2

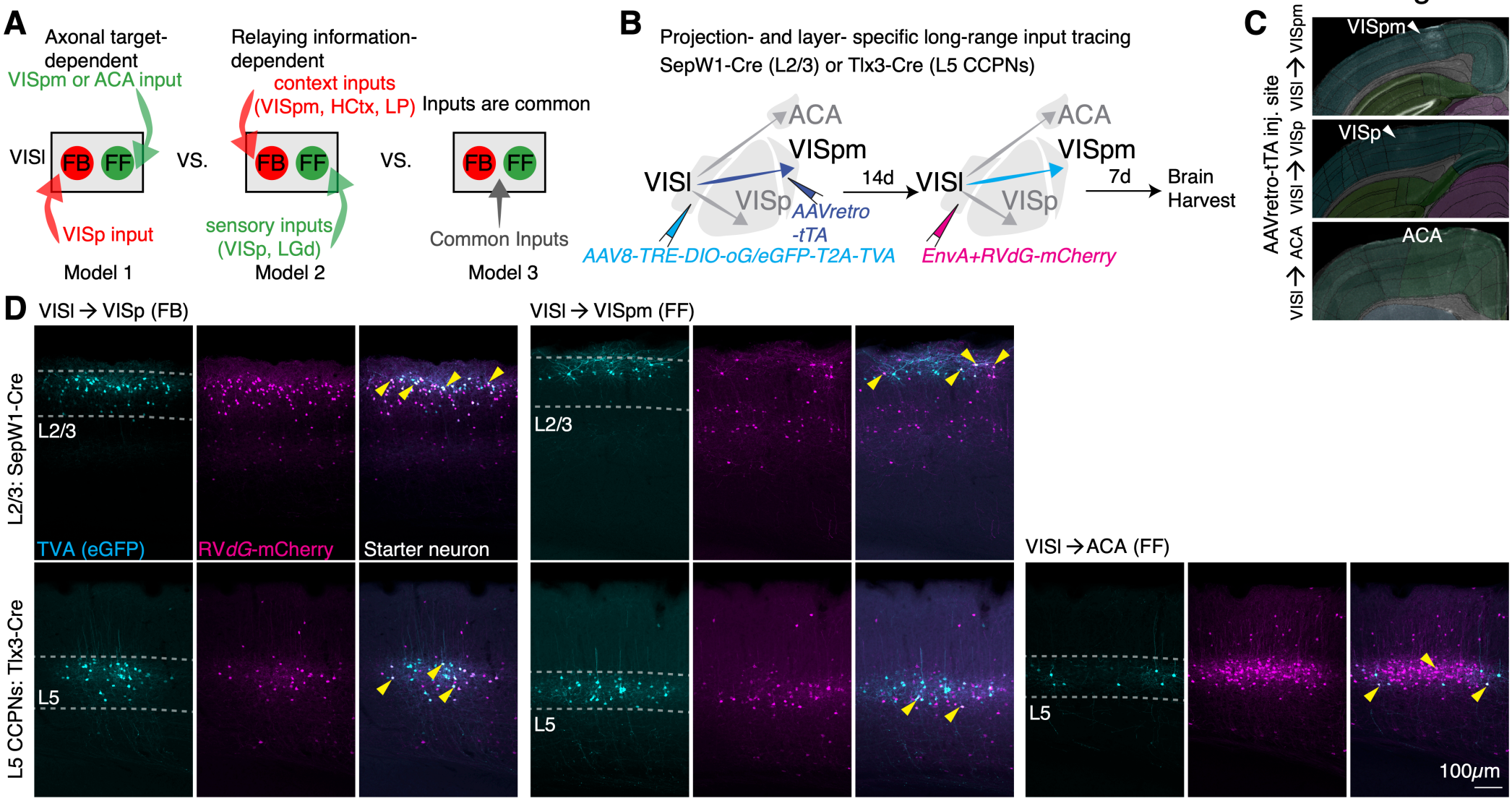
A
Axonal target-dependent
VISpm or ACA input
VISl
FB
FF
VISp input
Model 1
VS.
Relaying information-dependent
context inputs
(VISpm, HCtx, LP)
sensory inputs
(VISp, LGd)
Model 2
VS.
Inputs are common
Common Inputs
Model 3
B
Projection- and layer- specific long-range input tracing
SepW1-Cre (L2/3) or Tlx3-Cre (L5 CCPNs)
ACA
VISpm
VISl
VISp
AAVretro
-tTA
AAV8-TRE-DIO-oG/eGFP-T2A-TVA
14d
EnvA+RVdG-mCherry
7d
Brain
Harvest
C
AAVretro-tTA inj. site
VISl → VISpm
VISl → VISp
VISl → ACA
VISpm
VISp
ACA
D
VISl → VISp (FB)
VISl → VISpm (FF)
VISl → ACA (FF)
L2/3: SepW1-Cre
L5 CCPNs: Tlx3-Cre
L2/3
L5
TVA (eGFP)
RVdG-mCherry
Starter neuron
100μm

Figure 3

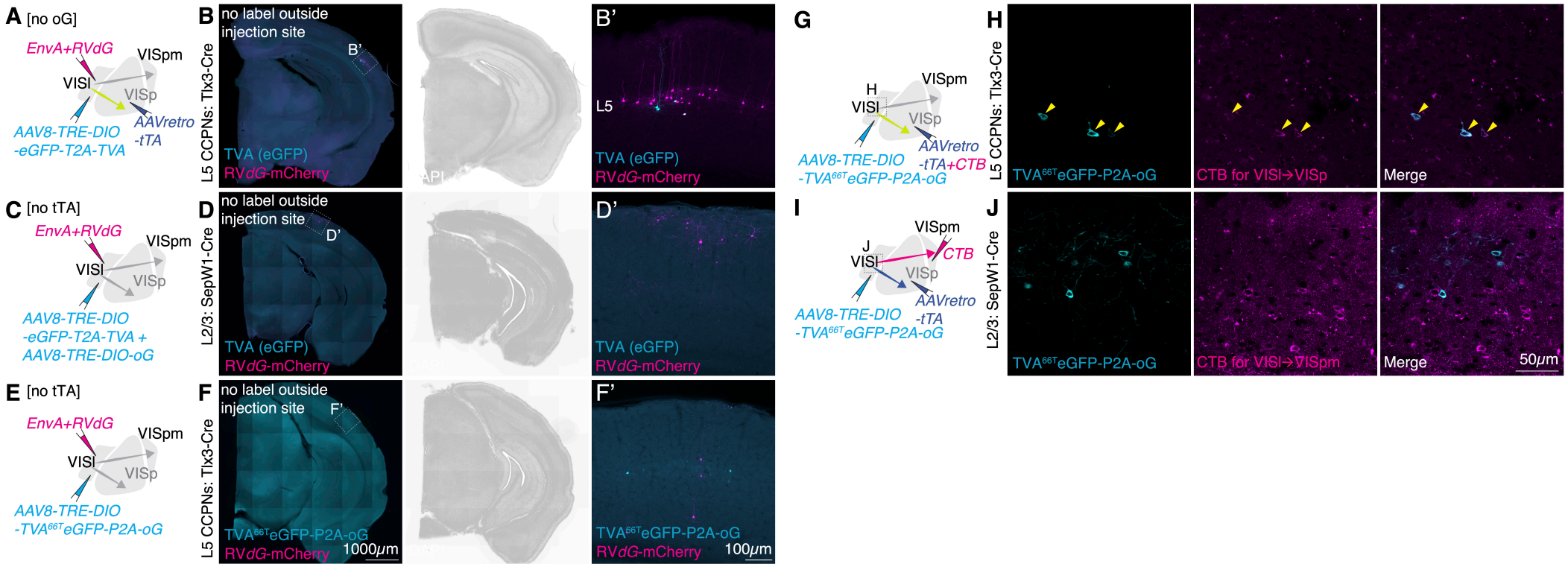
A [no oG]
EnvA+RVdG
VISpm
VISl
VISp
AAV8-TRE-DIO
-eGFP-T2A-TVA
AAVretro
-tTA
B
no label outside
injection site
B'
L5 CCPNs: Tlx3-Cre
TVA (eGFP)
RVdG-mCherry
L5
C [no tTA]
EnvA+RVdG
AAV8-TRE-DIO
-eGFP-T2A-TVA +
AAV8-TRE-DIO-oG
D
D'
L2/3: SepW1-Cre
E [no tTA]
AAV8-TRE-DIO
-TVA66TeGFP-P2A-oG
F
F'
TVA66TeGFP-P2A-oG
1000μm
100μm
G
H
AAVretro
-tTA+CTB
I
J
CTB
CTB for VISl→VISp
CTB for VISl→VISpm
Merge
50μm

Figure 4

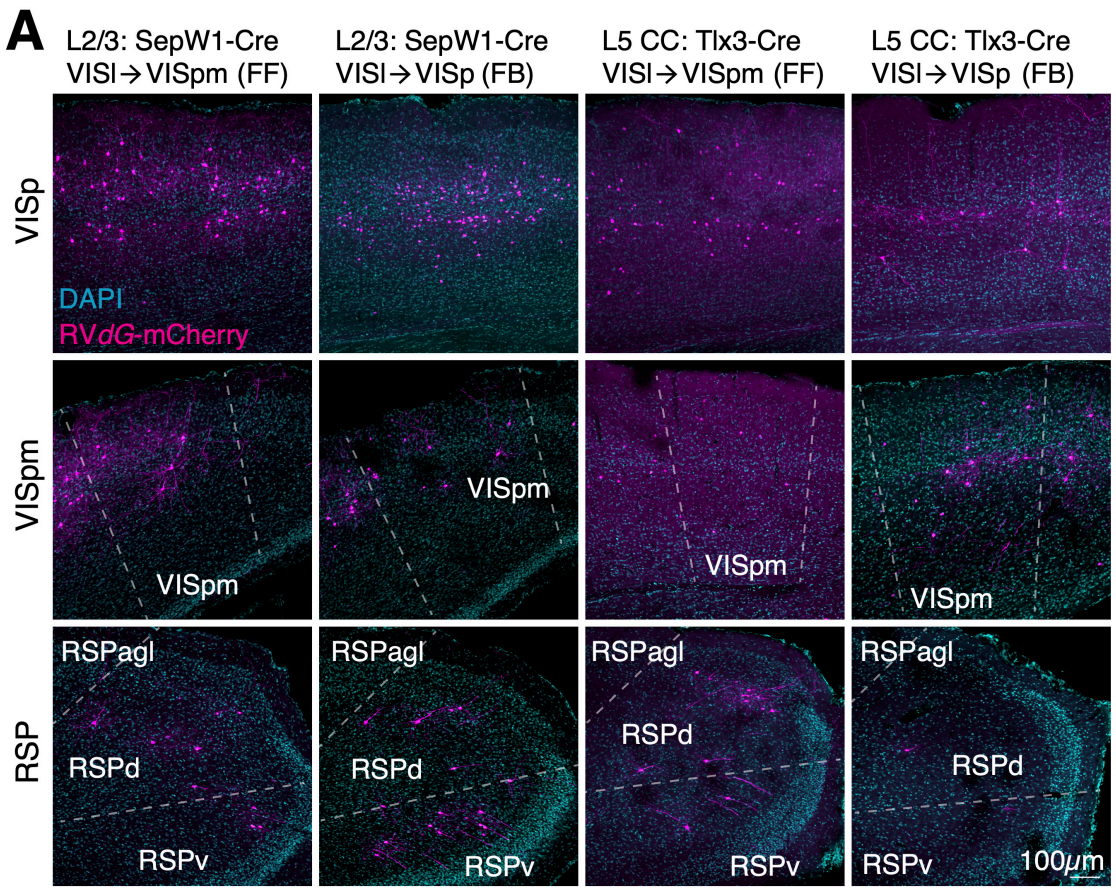
A
L2/3: SepW1-Cre
VISl→VISpm (FF)
L2/3: SepW1-Cre
VISl→VISp (FB)
L5 CC: Tlx3-Cre
VISl→VISpm (FF)
L5 CC: Tlx3-Cre
VISl→VISp (FB)
VISp
VISpm
RSP
DAPI
RVdG-mCherry
VISpm
RSPagl
RSPd
RSPv
100μm

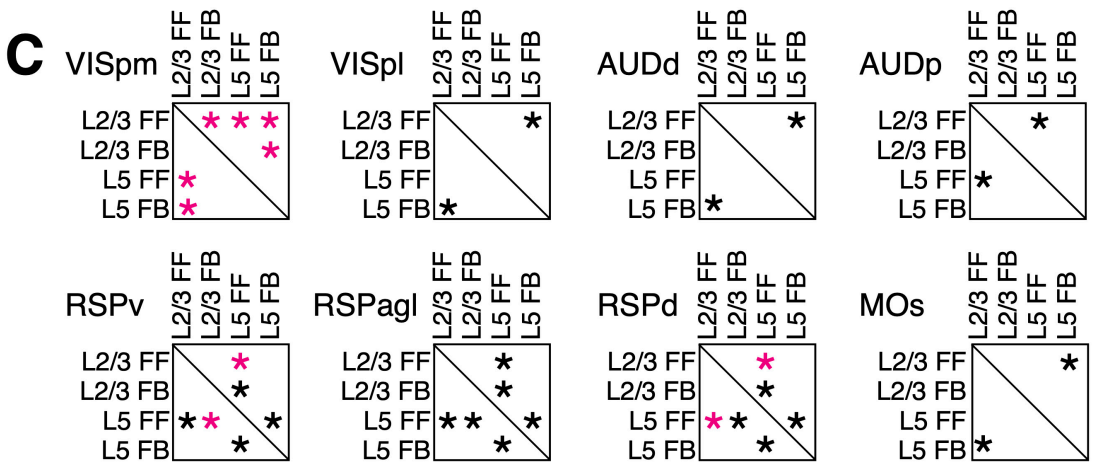
C
VISpm
VISpl
AUDd
AUDp
RSPv
RSPagl
RSPd
MOs
L2/3 FF
L2/3 FB
L5 FF
L5 FB

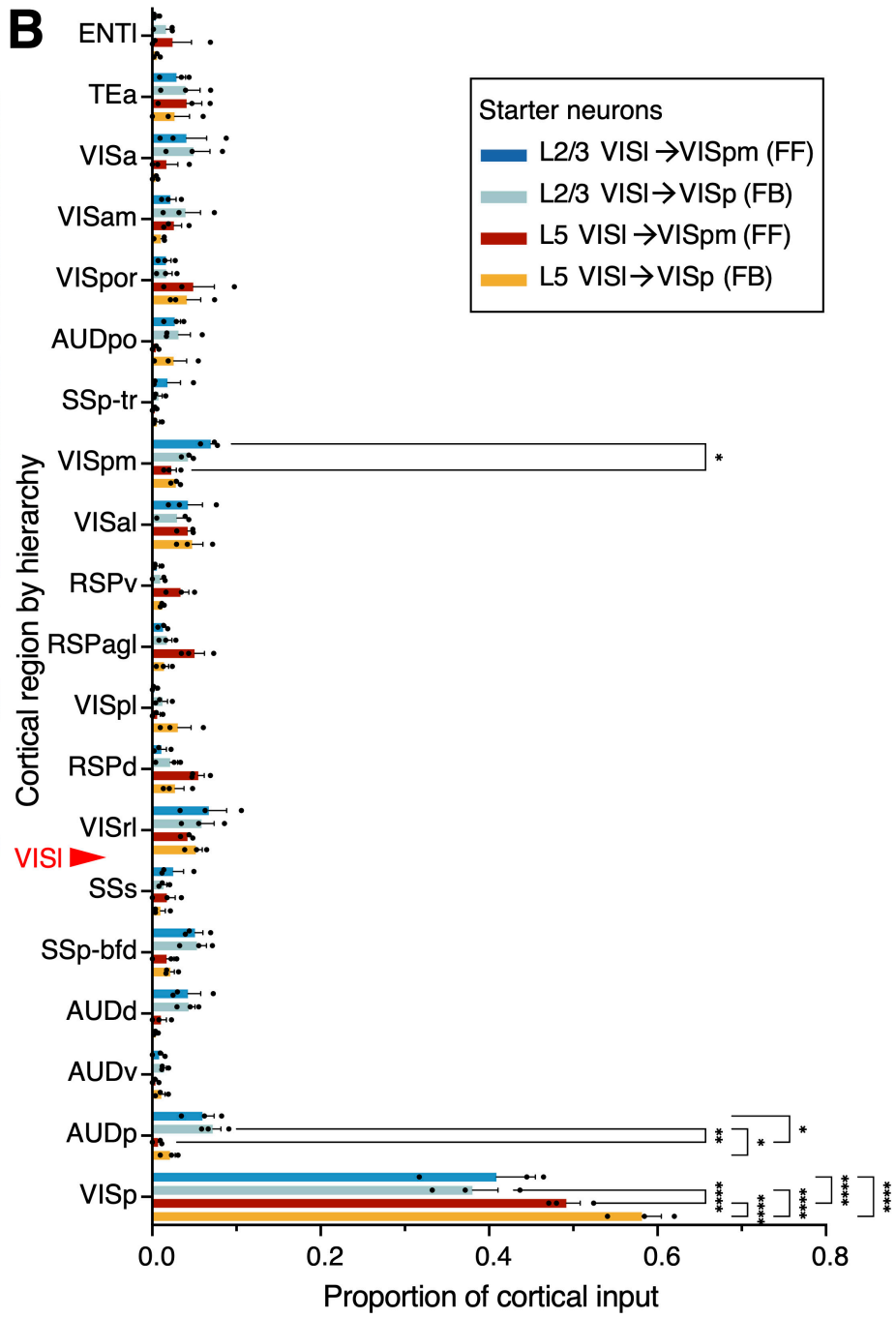
B
ENTl
TEa
VISa
VISam
VISpor
AUDpo
SSp-tr
VISpm
VISal
RSPv
RSPagl
VISpl
RSPd
VISrl
VISl
SSs
SSp-bfd
AUDd
AUDv
AUDp
VISp
Cortical region by hierarchy
Starter neurons
L2/3 VISl →VISpm (FF)
L2/3 VISl→VISp (FB)
L5 VISl →VISpm (FF)
L5 VISl→VISp (FB)
0.0
0.2
0.4
0.6
0.8
Proportion of cortical input

Figure 5

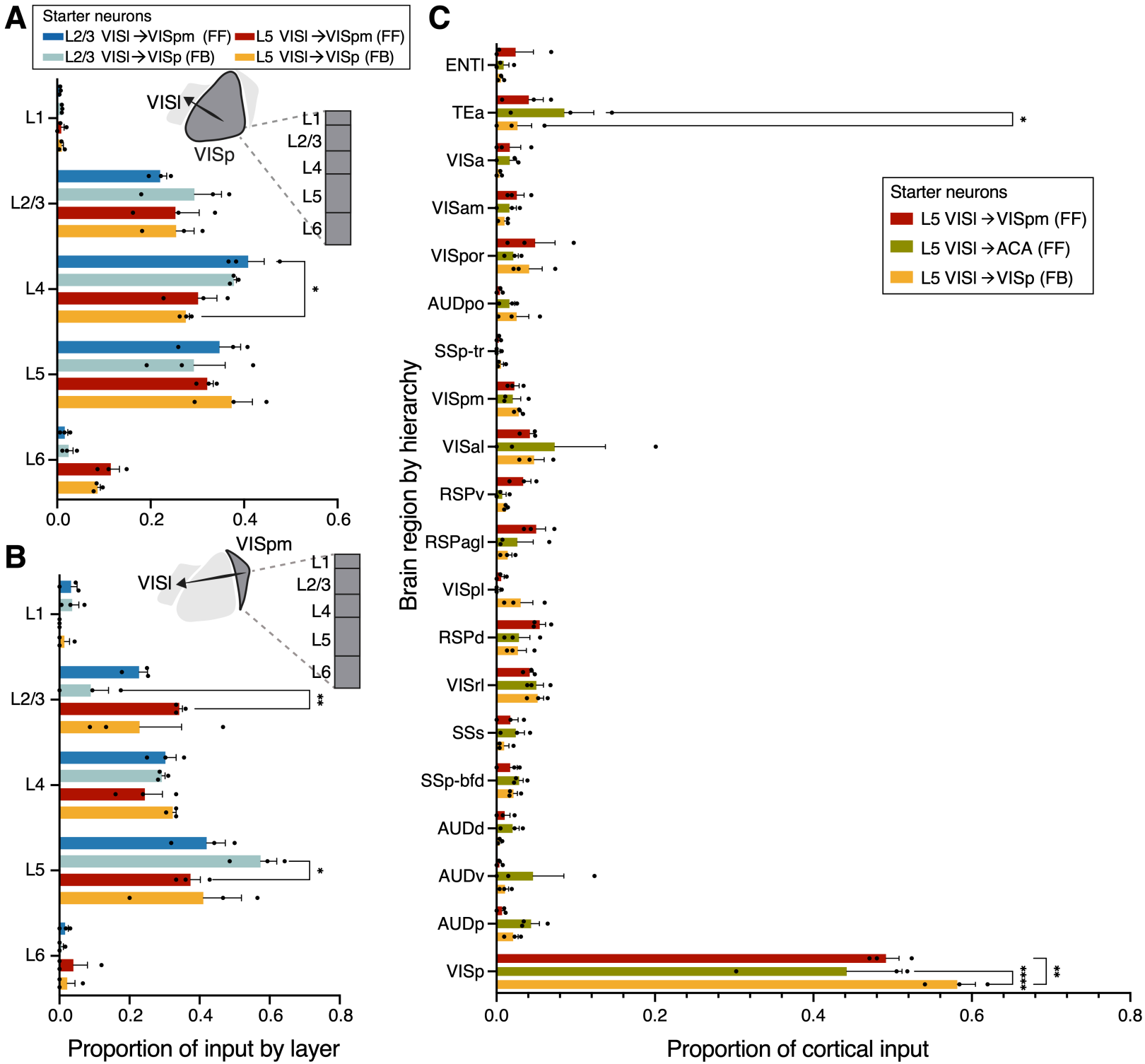
A
Starter neurons
L2/3 VISl →VISpm (FF)
L5 VISl →VISpm (FF)
L2/3 VISl→VISp (FB)
L5 VISl→VISp (FB)
VISl
VISp
L1
L2/3
L4
L5
L6
0.0
0.2
0.4
0.6
B
VISpm
VISl
0.8
Proportion of input by layer
C
ENTl
TEa
VISa
VISam
VISpor
AUDpo
SSp-tr
VISpm
VISal
RSPv
RSPagl
VISpl
RSPd
VISrl
SSs
SSp-bfd
AUDd
AUDv
AUDp
VISp
Brain region by hierarchy
Starter neurons
L5 VISl →VISpm (FF)
L5 VISl →ACA (FF)
L5 VISl →VISp (FB)
Proportion of cortical input

Figure 6

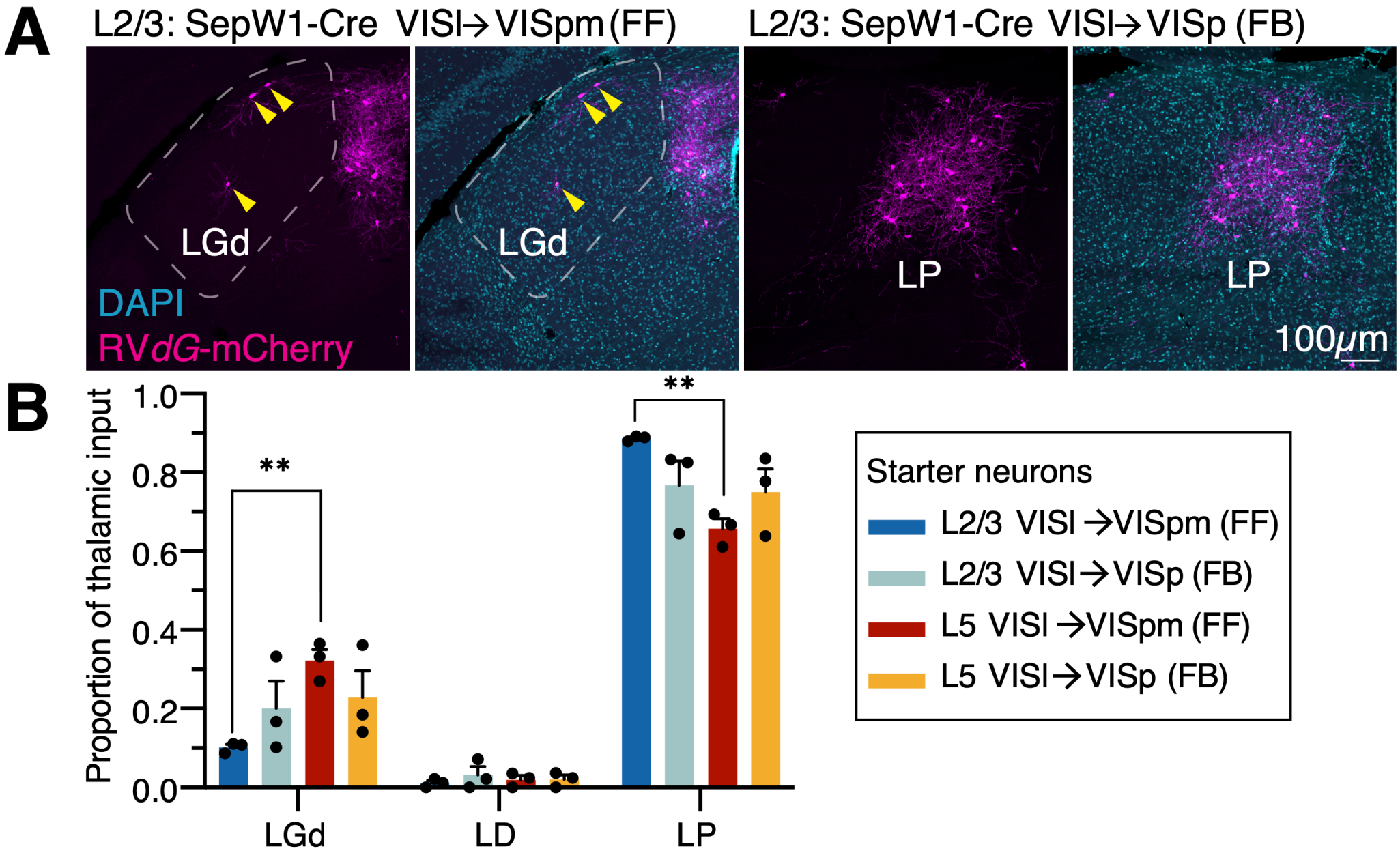
A
L2/3: SepW1-Cre VISl→VISpm (FF)
L2/3: SepW1-Cre VISl→VISp (FB)
LGd
LGd
LP
LP
DAPI
RVdG-mCherry
100μm
B
Proportion of thalamic input
1.0
0.8
0.6
0.4
0.2
0.0
**
**
LGd
LD
LP
Starter neurons
L2/3 VISl →VISpm (FF)
L2/3 VISl→VISp (FB)
L5 VISl →VISpm (FF)
L5 VISl→VISp (FB)